Article

Cell Chemical Biology

Exploiting polypharmacology to dissect host kinases and kinase inhibitors that modulate endothelial barrier integrity

Graphical abstract

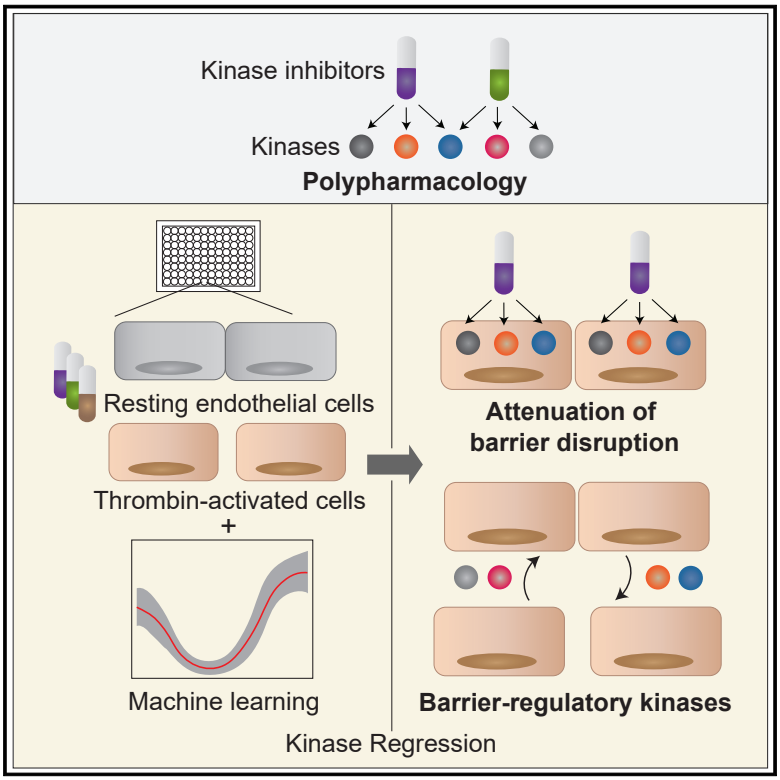

Highlights

- BCR-ABL drugs bosutinib, dasatinib, and imatinib have distinct barrier effects
- Polypharmacology influences the endothelial barrier activity of kinase inhibitors
- Kinase inhibitors can amplify or inhibit thrombin-mediated barrier disruption
- Several kinases in diverse pathways modulate endothelial barrier properties

Authors

Selasi Dankwa, Mary-Margaret Dols, Ling Wei, Elizabeth K.K. Glennon, Heather S. Kain, Alexis Kaushansky, Joseph D. Smith

Correspondence

alexis.kaushansky@seattlechildrens.org (A.K.), joe.smith@seattlechildrens.org (J.D.S.)

In brief

Dankwa et al. combine kinase inhibitor screens with a machine learning model to demonstrate that kinase inhibitors that target multiple kinases can strengthen and protect the endothelial barrier from proinflammatory, barrier-disruptive agents *in vitro*.

Dankwa et al., 2021, Cell Chemical Biology *28*, 1–14
December 16, 2021
https://doi.org/10.1016/j.chembiol.2021.06.004

CellPress

Cell Chemical Biology

CellPress

Article

Exploiting polypharmacology to dissect host kinases and kinase inhibitors that modulate endothelial barrier integrity

Selasi Dankwa,[1] Mary-Margaret Dols,[1] Ling Wei,[1] Elizabeth K.K. Glennon,[1] Heather S. Kain,[1] Alexis Kaushansky,[1,2,*] and Joseph D. Smith[1,2,3,*]

[1]Center for Global Infectious Disease Research, Seattle Children's Research Institute, Seattle, WA 98109, USA

[2]Department of Pediatrics, University of Washington, Seattle, WA 98105, USA

[3]Lead contact

*Correspondence: alexis.kaushansky@seattlechildrens.org (A.K.), joe.smith@seattlechildrens.org (J.D.S.)

https://doi.org/10.1016/j.chembiol.2021.06.004

SUMMARY

Kinase inhibitors are promising drugs to stabilize the endothelial barrier following inflammatory damage. However, our limited knowledge of how kinase signaling activates barrier-restorative pathways and the complexity of multi-target drugs have hindered drug discovery and repurposing efforts. Here, we apply a kinase regression approach that exploits drug polypharmacology to investigate endothelial barrier regulation. A screen of 28 kinase inhibitors identified multiple inhibitors that promote endothelial barrier integrity and revealed divergent barrier phenotypes for BCR-ABL drugs. Target deconvolution predicted 50 barrier-regulating kinases from diverse kinase families. Using gene knockdowns, we identified kinases with a role in endothelial barrier regulation and dissected different mechanisms of action of barrier-protective kinase inhibitors. These results demonstrate the importance of polypharmacology in the endothelial barrier phenotype of kinase inhibitors and provide promising new leads for barrier-strengthening therapies.

INTRODUCTION

Endothelial cells form a barrier between blood and tissue, maintaining selective permeability of the barrier, and participating in the inflammatory response (Aird, 2007; Pober and Sessa, 2007, 2015). During infection or injury, endothelial cells become activated by inflammatory stimuli from microbial or endogenous products, a state that allows them to appropriately participate in host repair and immune defense. However, excessive inflammation can lead to endothelial dysfunction, vascular leak, and tissue edema (Pober and Sessa, 2007). The loss of barrier control, coupled with thrombosis, can have dire consequences in diverse conditions, such as traumatic brain injury (Chang et al., 2016), ischemic stroke (Park-Windhol and D'Amore, 2016), sepsis (Levi and van der Poll, 2017), and malaria (Erice and Kain, 2019; Moxon et al., 2013). While endothelial dysfunction is implicated in numerous diseases, limited drugs exist to treat this condition. A more comprehensive understanding of the processes that regulate endothelial cell function could inform the development or repurposing of drugs that protect endothelial cells from excessive inflammation and repair vascular leak.

Endothelial barrier regulation is a complex process involving both barrier-disruptive and barrier-restorative signaling pathways (Komarova et al., 2007, 2017; Mehta and Malik, 2006; Radeva and Waschke, 2018). Barrier-disruptive pathways promote actin stress fiber formation and disassembly of inter-endothelial junctions, as well as loss of integrin-anchored focal adhesions that tether endothelial cells to the extracellular matrix. Barrier integrity is restored by barrier-enhancing pathways that lead to reassembly of inter-endothelial junctions, rearrangement of actin into cortical actin bundles, and strengthening of focal adhesions. The barrier-disruptive and barrier-restorative pathways are mediated in large part by kinases (Komarova et al., 2007, 2017; Kuppers et al., 2014; Mehta and Malik, 2006; Yuan, 2002). For instance, vascular endothelial (VE)-cadherin, the major protein of adherens junctions, is phosphorylated by c-Src, leading to internalization of VE-cadherin and destabilization of junctions in the presence of inflammatory mediators (Giannotta et al., 2013; Orsenigo et al., 2012; Wallez et al., 2007). The Src family kinases (SFKs), of which c-Src is a member, are also activated during barrier recovery following thrombin- and LPS-induced permeability (Birukova et al., 2013; Han et al., 2013; Klomp et al., 2019; Knezevic et al., 2009), and in response to barrier-strengthening mediators, such as sphingosine-1-phosphate (S1P) (Garcia et al., 2001; McVerry and Garcia, 2004; Vouret-Craviari et al., 2002). Thus, SFKs play a dual role in endothelial barrier permeability and restoration. The phosphoproteomic identification of more than 2,000 thrombin-regulated phosphorylation sites in human endothelial cells (van den Biggelaar et al., 2014) emphasizes the complexity of kinase regulation of endothelial barrier integrity.

Given the importance of phosphosignaling to barrier maintenance, kinase inhibition is an attractive approach to pursue as a barrier restoration and stabilization strategy (Glennon et al.,

Please cite this article in press as: Dankwa et al., Exploiting polypharmacology to dissect host kinases and kinase inhibitors that modulate endothelial barrier integrity, Cell Chemical Biology (2021), https://doi.org/10.1016/j.chembiol.2021.06.004

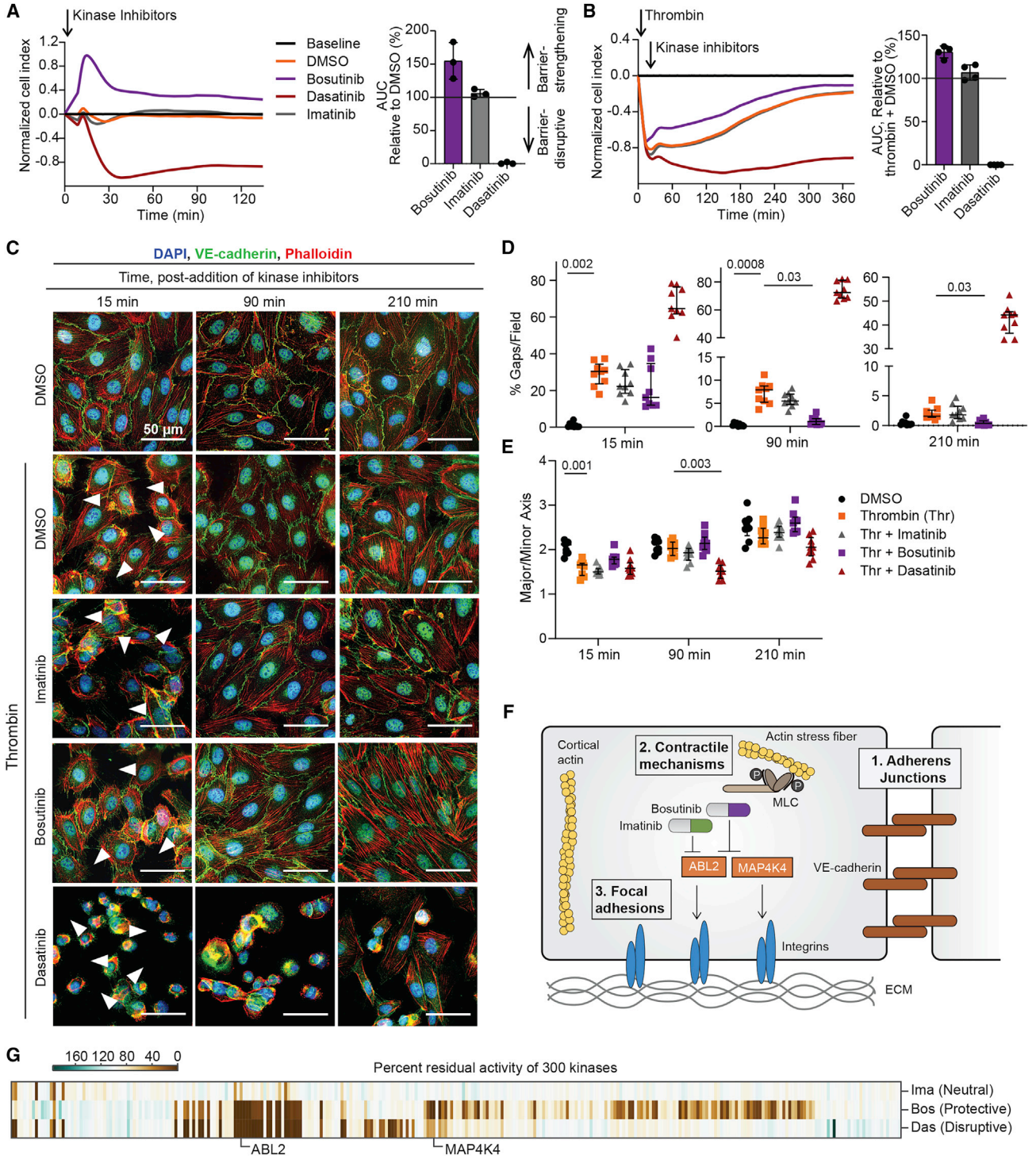

Figure 1. Three BCR-ABL-targeting kinase inhibitors with diverse polypharmacology have disparate effects on the HBMEC barrier

(A) Left: representative recordings from an xCELLigence assay showing the normalized cell index after addition of 0.5 µM bosutinib, dasatinib, and imatinib to resting HBMECs. Right: total change in cell index is summarized as area under the curve (AUC) relative to DMSO (100%): >100%, barrier strengthening; <100%, barrier disruption. Data are represented as mean ± SD of three independent experiments, each done in triplicate. See also Figure S1.

(B) Left: representative recordings from an xCELLigence assay showing the normalized cell index after addition of 0.5 µM bosutinib, dasatinib, and imatinib to HBMECs pre-treated with thrombin. Right: AUC quantification of xCELLigence assays. Data are represented as mean ± SD of four independent experiments, each in triplicate.

(A and B) Baseline: HBMECs exposed to medium only.

(legend continued on next page)

Please cite this article in press as: Dankwa et al., Exploiting polypharmacology to dissect host kinases and kinase inhibitors that modulate endothelial barrier integrity, Cell Chemical Biology (2021), https://doi.org/10.1016/j.chembiol.2021.06.004

2018; Rizzo et al., 2015). Recent evidence indicates that the BCR-ABL-targeting kinase inhibitors, imatinib (Gleevec) and bosutinib (Bosulif), attenuate vascular leakage in a murine model of sepsis and acute lung injury, respectively (Aman et al., 2012; Botros et al., 2020). The protective activities of imatinib and bosutinib, which include strengthening of focal adhesions and promoting junctional integrity, have been attributed to inhibition of Abelson homolog 2 (ABL2; also known as ARG) in the case of imatinib, and ABL2 and mitogen-activated protein 4 kinase 4 (MAP4K4) in the case of bosutinib (Aman et al., 2012; Botros et al., 2020). With over 60 kinase inhibitors approved for clinical use and more than 200 in clinical testing (Klaeger et al., 2017; Roskoski, 2021), there are many opportunities for drug repurposing. A challenge of kinase inhibitors is drug polypharmacology, where a single drug acts on multiple kinases, both intended and off-target (Reddy and Zhang, 2013). Here, we exploit the polypharmacology of kinase inhibitors using a systems-based approach known as kinase regression (KiR) (Arang et al., 2017; Gujral et al., 2014) to identify kinases that regulate endothelial barrier properties and to explore how drug polypharmacology influences barrier phenotypes.

RESULTS

Three BCR-ABL-targeting kinase inhibitors with diverse polypharmacology have disparate effects on the human brain microvascular endothelial cell barrier

Of the BCR-ABL class of kinase inhibitors, imatinib and bosutinib have been shown to attenuate vascular leakage (Aman et al., 2012; Botros et al., 2020; Rizzo et al., 2015), while dasatinib is barrier disruptive (Botros et al., 2020; Fazakas et al., 2018; Han et al., 2013). To investigate these divergent phenotypes, we compared bosutinib, imatinib, and dasatinib against primary human brain microvascular endothelial cells (HBMECs). We monitored changes in the HBMEC barrier using the xCELLigence system, which measures electrode impedance across cells and reports a cell index—a proxy for the strength of cell-cell interactions and cell adhesion to the substrate.

The three BCR-ABL kinase inhibitors had diverse phenotypes as indicated by the dynamics of the xCELLigence traces and the area under the curve (AUC) (Figures 1A and S1A). Under resting conditions, bosutinib strengthened the barrier and dasatinib was barrier disruptive, as previously reported (Botros et al., 2020; Fazakas et al., 2018; Han et al., 2013) (Figure 1A). In contrast, imatinib had little effect (Figure 1A). The effects of bosutinib and dasatinib were dose dependent (Figure S1B), indicating a robustness of their distinct barrier phenotypes. To study the effect of the kinase inhibitors on activation of HBMECs by thrombin (a proinflammatory and barrier-disruptive stimulus), thrombin was given 6–9 min before the kinase inhibitors, at which point barrier disruption was already under way. Under thrombin-activated conditions, bosutinib and dasatinib again had opposing effects; bosutinib attenuated thrombin-induced barrier disruption in a dose-dependent manner and dasatinib exacerbated it (Figures 1B, S1C, and S1D). Imatinib had little effect. Consistent with these results, immunofluorescence images stained for a molecular marker of adherens junctions (VE-cadherin) and the actin cytoskeleton, indicated fewer gaps per field at all time points in thrombin-stimulated cells treated with bosutinib and imatinib compared with dasatinib (Figures 1C–1E). In addition, bosutinib-treated cells recovered more rapidly than imatinib-treated cells and had fewer gaps than imatinib-treated cells and the thrombin + DMSO control at the 90- and 210-min time points (Figures 1C–1E). Conversely, dasatinib dramatically exacerbated thrombin-mediated permeability by inducing extreme cell retraction, perinuclear staining of VE-cadherin and actin, and delaying recovery of cell shape (Figures 1C–1E). We confirmed that the barrier-disruptive effect of dasatinib was not the result of cell death (Figures S1E and S1F). Overall, microscopic analysis supported the xCELLigence data and reinforced the opposing barrier activities of bosutinib and dasatinib, despite being in the same family of drugs.

There are three main ways by which endothelial cells regulate barrier properties, namely via cell-cell junctions (including adherens junctions), contractile mechanisms (involving remodeling of the actin cytoskeleton), and cell-matrix interactions (including focal adhesions) (Figure 1F). The protective effect of bosutinib and imatinib has been linked to regulation of focal adhesions and cell-cell junctions through inhibition of MAP4K4 and/or ABL2 (Aman et al., 2012; Botros et al., 2020). However, both kinases are also inhibited by dasatinib (barrier disruptive) (Anastassiadis et al., 2011). In addition, bosutinib and dasatinib inhibited 58 kinases and 48 kinases, respectively, by 70% or more (Anastassiadis et al., 2011) (Figure 1G). This extensive polypharmacology suggests that off-target inhibition and pleiotropic activity on multiple kinases may explain the disparate activities of bosutinib, imatinib, and dasatinib.

Multiple kinase inhibitors alter endothelial barrier integrity under resting and activated conditions

To study how polypharmacology may influence drug activity, we used KiR (Gujral et al., 2014). KiR uses the results of a small-scale screen of kinase inhibitors with partially overlapping targets to deconvolve and predict kinases that are informative for a specific phenotype (Anastassiadis et al., 2011; Gujral et al., 2014) (Figure 2A). Kinase predictions are made using a machine

(C) Immunofluorescence images at 15, 90, and 210 min after addition of 0.5 μM imatinib, bosutinib, and dasatinib to thrombin-treated HBMECs. Cells are labeled with anti-VE-cadherin (green), phalloidin (red), and DAPI (blue). Shown are representative images from one of three independent experiments. Arrowheads highlight gaps. Scale bars: 50 μm.

(D and E) ImageJ quantification of immunofluorescence images showing intercellular gaps per field (D) and cell aspect ratio (major/minor axis) (E). Three fields were quantified per condition from three independent experiments. Bars indicate the median and interquartile range. Statistical significance between thrombin and all other groups was evaluated using Kruskal-Wallis and Dunn's multiple comparison test.

(F) Diagram illustrating the three principal means of endothelial barrier regulation. Two targets of bosutinib and imatinib implicated in their barrier-strengthening activity (ABL2 and MAP4K4) are highlighted.

(G) Heatmap showing the residual biochemical kinase activity after inhibition of each of 300 kinases by 0.5 μM imatinib, bosutinib, and dasatinib. The data are from Anastassiadis et al. (2011). ABL2 and MAP4K4 are highlighted.

Please cite this article in press as: Dankwa et al., Exploiting polypharmacology to dissect host kinases and kinase inhibitors that modulate endothelial barrier integrity, Cell Chemical Biology (2021), https://doi.org/10.1016/j.chembiol.2021.06.004

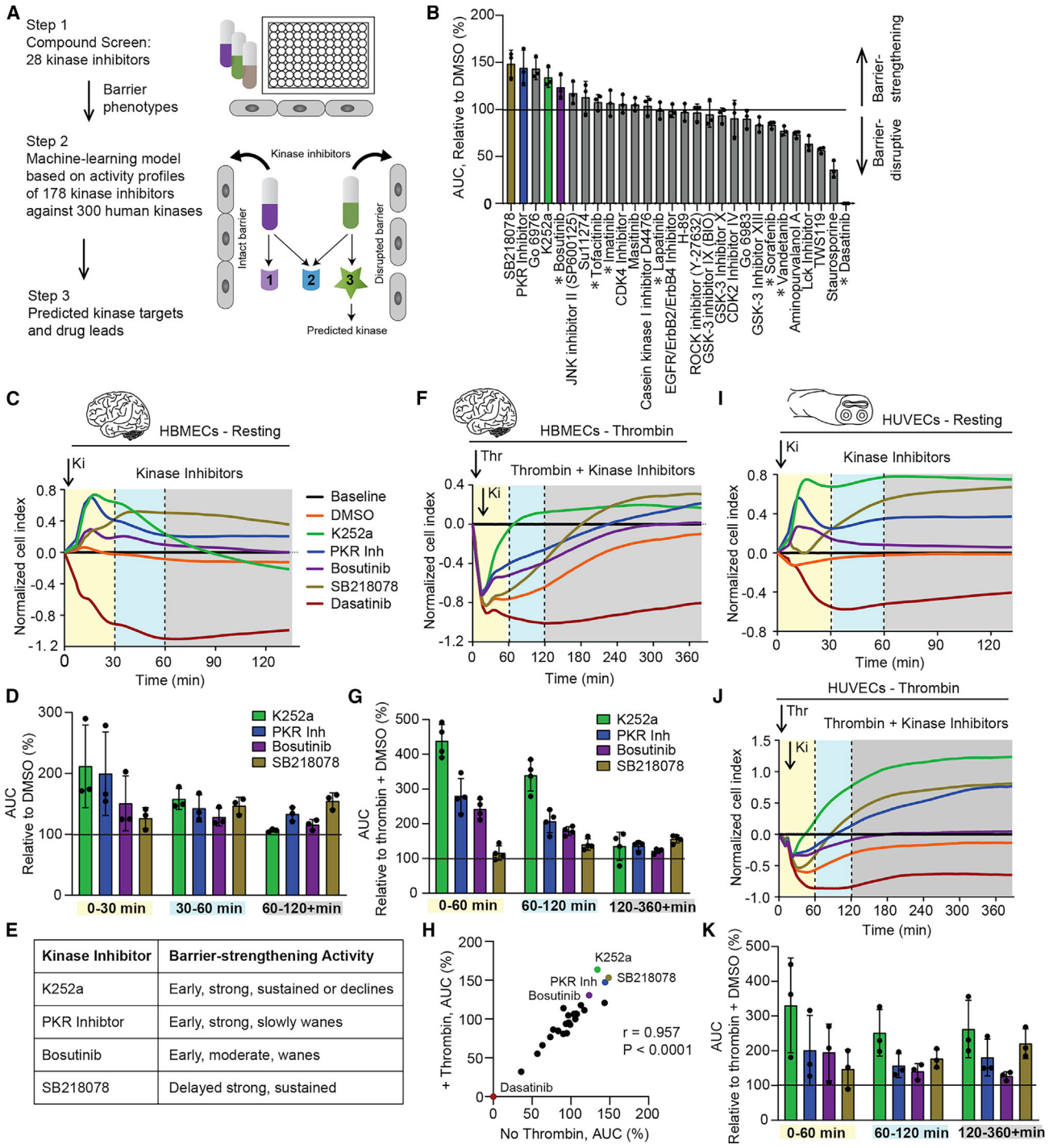

Kinase Inhibitor	Barrier-strengthening Activity
K252a	Early, strong, sustained or declines
PKR Inhibtor	Early, strong, slowly wanes
Bosutinib	Early, moderate, wanes
SB218078	Delayed strong, sustained

Figure 2. Multiple kinase inhibitors alter endothelial barrier integrity under resting and activated conditions

(A) Steps involved in kinase regression approach.

(B) AUC quantification of xCELLigence kinase inhibitor screens performed at 0.5 μM in resting HBMECs. Shown is the mean ± SD of three independent experiments, each in triplicate. Asterisks indicate kinase inhibitors in human clinical use. See also Table S1 and Data S1.

(C) Representative recordings from xCELLigence kinase inhibitor screen in resting HBMECs.

(D) Temporal AUC analysis of resting HBMECs + kinase inhibitors.

(E) Description of the temporal barrier-strengthening activity of four kinase inhibitors.

(F) Representative recordings from xCELLigence screen in HBMECs treated with thrombin followed by 0.5 μM kinase inhibitors. See also Figure S2.

(G) Temporal AUC analysis of HBMECs treated with thrombin followed by kinase inhibitors.

(legend continued on next page)

Please cite this article in press as: Dankwa et al., Exploiting polypharmacology to dissect host kinases and kinase inhibitors that modulate endothelial barrier integrity, Cell Chemical Biology (2021), https://doi.org/10.1016/j.chembiol.2021.06.004

learning model, which is based on the residual activity of kinases after treatment with kinase inhibitors. We screened primary HBMECs with 28 kinase inhibitors, including bosutinib, imatinib, dasatinib, and four additional kinase inhibitors in human clinical use (lapatinib, sorafenib, tofacitinib, and vandetanib) (Table S1). The 28 kinase inhibitors have broad and partially overlapping kinase specificity to inform the machine learning predictions (Anastassiadis et al., 2011; Gujral et al., 2014).

Like bosutinib, the kinase inhibitors K252a, RNA-dependent protein kinase (PKR) inhibitor, and SB 218078 had a barrier-strengthening effect, causing the cell index to rise significantly above baseline (Figures 2B and 2C). Other kinase inhibitors, such as TWS119 and staurosporine, caused a significant drop in the cell index indicative of a barrier-disruptive effect (Figures 2B and 2C), although the effects of staurosporine could be partially attributed to apoptosis (Figures S1E and S1F). Many kinase inhibitors did not alter barrier properties (Figure 2B). Among the barrier-strengthening kinase inhibitors, we observed varying patterns of cell index changes (Figure 2C), which were quantified by measuring the AUC across three time blocks (Figure 2D). K252a, PKR inhibitor, and bosutinib had an early barrier-strengthening effect with a peak cell index within the first 30 min. However, they differed in the extent and decline of barrier strengthening (Figures 2D and 2E). By comparison, SB 218078 had a delayed barrier-strengthening effect that built gradually over the first 30 min and then was sustained (Figures 2D and 2E). The varying temporal dynamics suggest different mechanisms of action.

Next, we assessed the 28 kinase inhibitors on HBMECs pretreated with thrombin for 6–9 min ahead of the kinase inhibitors. There were striking similarities in the classification of barrier-strengthening and barrier-protective kinase inhibitors under resting and thrombin-activated conditions (Figures 2B and S2A) in both AUC measurements of kinase activity as well as the rate of recovery to baseline (Figures S2A and S2B). The two exceptions were glycogen synthase kinase 3 (GSK-3) inhibitor IX (BIO) and cyclin-dependent kinase 2 (CDK2) inhibitor IV; neither perturbed the barrier under resting conditions; however, GSK-3 inhibitor IX exacerbated thrombin-induced barrier disruption, while CDK2 inhibitor IV was barrier protective under thrombin challenge (Figures 2B and S2A).

We found that barrier-strengthening kinase inhibitors either blunted thrombin's barrier-disruptive effect and/or increased the rate of barrier recovery back to baseline, relative to thrombin + DMSO-treated cells (Figures 2F and 2G). The activity of K252a, PKR inhibitor, SB 218078, and bosutinib on thrombin-activated HBMECs mirrored their temporal activity on resting HBMECs. When added to thrombin-treated cells, K252a, PKR inhibitor, and bosutinib rapidly halted the descent of the cell index, consistent with the early barrier-strengthening effect of these kinase inhibitors under resting conditions (Figures 2C and 2F). In addition, K252a promoted faster recovery of the endothelial barrier (Figure 2F). Conversely, SB 218078, with its delayed activity, had a negligible effect on the extent of thrombin-induced barrier disruption but promoted faster recovery of the barrier to baseline (Figure 2F). In a second experimental design, the four barrier-protective kinase inhibitors were given a 15-min head start before addition of thrombin. Pretreatment of HBMECs with the four protective kinase inhibitors blunted, but did not eliminate, the barrier-disruptive effect of thrombin (Figure S2C). Together, the observed barrier-strengthening activity on resting cells and barrier-protective activity on thrombin-perturbed cells are reminiscent of natural products, such as S1P, that have physiological roles in barrier restoration after inflammation (Garcia et al., 2001). Conversely, barrier-disruptive kinase inhibitors, such as dasatinib, exacerbated thrombin-induced barrier disruption and prolonged barrier recovery. The strong correlation between kinase inhibitor phenotypes under resting and thrombin-activated states (Pearson $r = 0.957$, $p < 0.0001$; Figure 2H) suggests that, under both cellular conditions, the kinase inhibitors may engage similar signaling pathways.

A subset of kinase inhibitors were tested on resting and thrombin-activated primary human umbilical vein endothelial cells (HUVECs). HUVECs had a similar response as HBMECs to K252a, SB 218078, PKR inhibitor, bosutinib, and dasatinib, except that the effect of K252a on resting HUVECs was sustained (Figures 2I and 2J). Moreover, the temporal activity of the four barrier-strengthening kinase inhibitors, K252a, PKR inhibitor, SB 218078, and bosutinib, followed a similar trend (Figures 2I–2K). Overall, there was a remarkably high correlation between the response of HUVECs and HBMECs to the five kinase inhibitors in the presence and absence of thrombin.

Kinase inhibition modulates HBMEC barrier integrity under proinflammatory conditions

To gain additional mechanistic insight into kinase inhibitor activity, we assessed changes in the thrombin-treated HBMEC barrier by monitoring VE-cadherin and actin. At the 15-min time point, K252a had already substantially inhibited and repaired gaps induced by thrombin ($p = 0.0001$, Thr + DMSO versus Thr + K252a), compared with the slower-acting SB 218078 (Figures 3A and 3B). At 90 min, while gaps remained in thrombin-treated HBMECs, there were virtually none in cells treated with K252a ($p < 0.0001$) and SB 218078 ($p = 0.001$), and only a small percent in monolayers treated with PKR inhibitor (Figures 3A and 3B). Interestingly, the cell aspect ratio of thrombin- and SB 218078-treated cells was smaller in comparison with DMSO-treated cells and K252a-treated cells at 15 min, indicating a roundness associated with cell retraction that reflects the extent of gap formation (Figure 3C). Altogether, the microscopy findings and the xCELLigence analysis underscored the differential

(H) Correlation between the AUC of kinase inhibitor-treated HBMECs in the resting state or with thrombin activation. The Pearson correlation coefficients and associated p values are indicated.

(I and J) Representative recordings from xCELLigence assays with HUVECs treated with 0.5 μM kinase inhibitors under resting conditions (I) and after thrombin treatment (J).

(K) Temporal AUC analysis of HUVECs treated with thrombin, then kinase inhibitors.

(C, F, I, and J) Baseline: cells exposed to medium only. (D, G, and K) Data are represented as mean ± SD of three (D and K) or four (G) independent experiments, each in triplicate.

Please cite this article in press as: Dankwa et al., Exploiting polypharmacology to dissect host kinases and kinase inhibitors that modulate endothelial barrier integrity, Cell Chemical Biology (2021), https://doi.org/10.1016/j.chembiol.2021.06.004

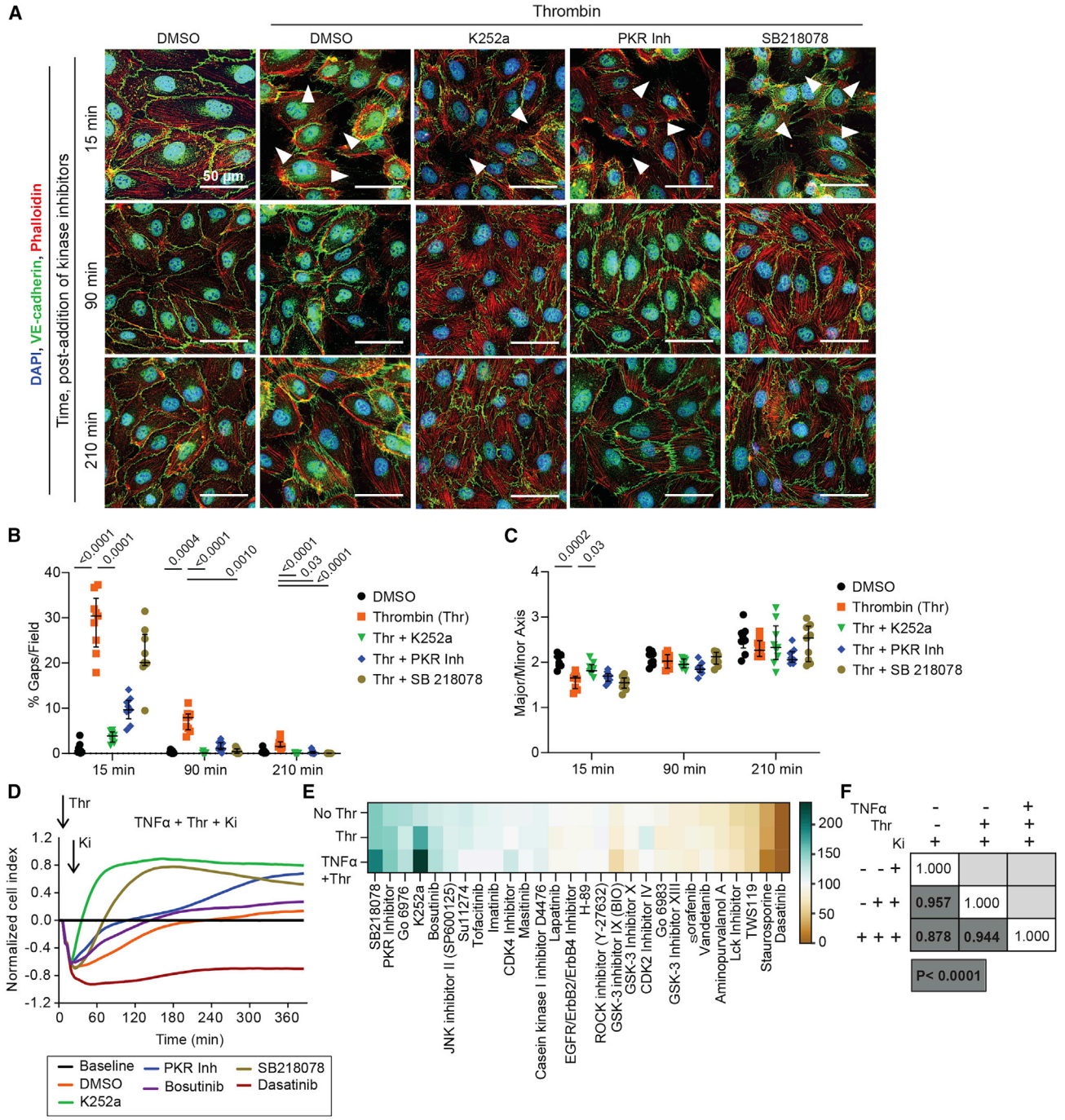

Figure 3. Kinase inhibition modulates HBMEC barrier integrity under proinflammatory conditions

(A) Representative images of thrombin-treated HBMECs at 15, 90, and 210 min after addition of 0.5 μM kinase inhibitors. Cells are labeled with anti-VE-cadherin (green), phalloidin (red), and DAPI (blue). Arrowheads highlight gaps. Scale bars: 50 μm. Images are representative of three independent experiments and are from the same experiment in Figure 1C.

(B and C) Quantification of images of thrombin-treated HBMECs at 15, 90, and 210 min after addition of 0.5 μM kinase inhibitors showing intercellular gaps per field (B) and cell aspect ratio (major/minor axis; C). The median and interquartile range are shown. Three fields were analyzed per condition in each of three experiments. Statistical significance between thrombin and all other groups was evaluated using Kruskal-Wallis and Dunn's multiple comparison tests. Data for DMSO and thrombin control groups are identical to that in Figures 1D and 1E.

(legend continued on next page)

Please cite this article in press as: Dankwa et al., Exploiting polypharmacology to dissect host kinases and kinase inhibitors that modulate endothelial barrier integrity, Cell Chemical Biology (2021), https://doi.org/10.1016/j.chembiol.2021.06.004

temporal dynamics and activities of the protective kinase inhibitors on the HBMEC barrier.

The inflammatory cytokine tumor necrosis factor alpha (TNF-α) is often increased in vascular inflammatory diseases (Levi and van der Poll, 2010, 2017). Therefore, we assessed kinase inhibition in HBMECs in the context of TNF-α pretreatment. HBMECs treated with TNF-α + thrombin responded similarly to HBMECs treated with thrombin only (Figures 3D, 3E, 2F, 2G, S2A, and S2D). K252a, SB 218078, PKR inhibitor, and bosutinib were strongly barrier protective, while dasatinib was the most barrier-disruptive kinase inhibitor tested. Furthermore, like thrombin-treated HBMECs, but unlike resting HBMECs, GSK-3 inhibitor IX (BIO) exacerbated thrombin-induced barrier disruption. However, under TNF-α activation, but not in other conditions, CDK4 inhibitor was barrier protective. Overall, there was a strong correlation of HBMEC responses to the 28 kinase inhibitors under resting and inflammatory conditions with thrombin alone or in combination with TNF-α (Figures 3F and S2E). The barrier phenotypes of the seven kinase inhibitors in human clinical use were consistent across the different conditions and ranged from protective (bosutinib) or weakly protective/neutral (imatinib, tofacitinib), to weakly disruptive (lapatinib, sorafenib, and vandetanib) or strongly barrier disruptive (dasatinib) (Figure 3E).

KiR identifies kinases that are important in HBMEC barrier regulation

The data from the 28-kinase inhibitor screens of resting and activated HBMECs (Data S1) were used to train the KiR machine learning model (Figure 2A; Data S2; see also supplemental information), which predicted 50 kinases from a pool of 300 kinases as important in regulating HBMEC barrier properties (Figures 4A and 4C; Table S2). Some kinases were predicted to play a role under multiple conditions, others under a single condition. Unsupervised hierarchical clustering of the residual activity of the 50 predicted kinases against the 28 kinase inhibitors (Anastassiadis et al., 2011) revealed four clusters that largely separated barrier-disruptive kinase inhibitors (cluster 3, Figures 4A and 4B) from barrier-protective kinase inhibitors (cluster 4, Figures 4A and 4B). Interestingly, bosutinib clustered separately from the other barrier-protective kinase inhibitors. Nevertheless, many of the kinases targeted by the barrier-protective kinase inhibitors in cluster 4 were also inhibited by bosutinib (Figure 4A). The barrier-disruptive inhibitor staurosporine was also present in cluster 4 and shared kinase targets with both barrier-disruptive and barrier-strengthening inhibitors (Figure 4A), suggesting that the complex combinatorial action of kinase inhibitors determined their barrier phenotypes. In a similar vein, ABL2 was strongly inhibited by both barrier-protective (e.g., bosutinib) and barrier-disruptive (e.g., dasatinib, staurosporine) kinase inhibitors (Figure 4A), reinforcing that there were non-additive effects on barrier phenotypes, as has been observed from growth factor signaling (Janes et al., 2005).

Notably, 20 (40%) of the predicted kinases had previous evidence for involvement in endothelial barrier regulation (Figures 4D; Table S2). Several of these could be classified according to the barrier regulatory process they are implicated in, with some kinases, such as TGFBR1, being found in more than one category (contractile mechanisms, positive regulation of stress fibers, and VE-cadherin-associated; Figure 4D). Of the 50 predicted kinases, 30 had no previous association to endothelial barrier regulation (Figures 4D; Table S2), illustrating the discovery potential of KiR.

The multiplicity of kinase targets implicates a broad range of kinase signaling pathways in endothelial barrier regulation. As specific examples, the KiR model predicted multiple informative kinases in the RAF pathway and the signaling hub centered on LIMK1, a kinase involved in the positive regulation of actin stress fibers (Figure 4E). In addition, megakaryocyte-associated tyrosine kinase (MATK; also known as CHK or CTK), one of two negative regulators of SFKs known to mediate both barrier-protective and barrier-disruptive pathways (Chong et al., 2005; Okada, 2012), was predicted under all conditions tested (Figures 4E; Table S2).

Multiple uncharacterized kinases contribute to endothelial barrier integrity

We selected 11 kinases to validate by lentiviral-mediated short hairpin RNA (shRNA) knockdown (Figure 5A; Table S3). Five kinases, serine/threonine-protein kinase A-Raf (ARAF), calcium/calmodulin-dependent protein kinase IV (CAMK4), Never in mitosis A-related kinase 11 (NEK11), serine/arginine-rich protein-specific kinase 2 (SRPK2), and MATK have not previously been shown to be involved in endothelial barrier regulation. Furthermore, MATK was predicted to be important under all conditions tested (Table S2). While not predicted, we included C-terminal Src kinase (CSK) because together with MATK it negatively regulates SFKs (Chong et al., 2005; Okada, 2012), a gene family that has been implicated in both barrier-disruptive and barrier-restorative pathways. Similarly, Nemo-like kinase (NLK) was included because it is a negative regulator of the Wnt/β-catenin signaling pathway, which has been implicated in regulation of brain endothelial barrier integrity (Gallego-Delgado et al., 2016). In addition, we selected ephrin type-A receptor 4 (EPHA4) because it was previously reported to regulate barrier properties (Woodruff et al., 2016). The last three kinases, serine/threonine-protein kinase MRCK alpha, G protein-coupled receptor kinase 2 (GRK2/ADRBK1), and serine/threonine-protein kinase B-Raf (BRAF) are known to be involved in barrier regulatory processes, but have not been investigated in HBMECs. Of the three kinases, BRAF is the best characterized; ablation of endothelial BRAF in mice attenuates VEGF-induced barrier permeability *in vivo* and *in vitro* by promoting the formation of barrier strengthening cortical actin and stabilizing adherens junctions (Dorard et al., 2019).

(D) Representative recordings from xCELLigence 0.5 μM kinase inhibitor screen in TNF-α-activated HBMECs treated with thrombin. Baseline: cells exposed to medium only. See also Figure S2.

(E) Heatmap showing median AUC values from three to four xCELLigence kinase inhibitor screens (each in triplicate) in the resting state or with thrombin ± TNF-α activation.

(F) Pearson correlation coefficients and the associated p values are shown for a comparison of the AUC of kinase inhibitor-treated HBMECs in the resting state and with thrombin ± TNF-α activation.

Please cite this article in press as: Dankwa et al., Exploiting polypharmacology to dissect host kinases and kinase inhibitors that modulate endothelial barrier integrity, Cell Chemical Biology (2021), https://doi.org/10.1016/j.chembiol.2021.06.004

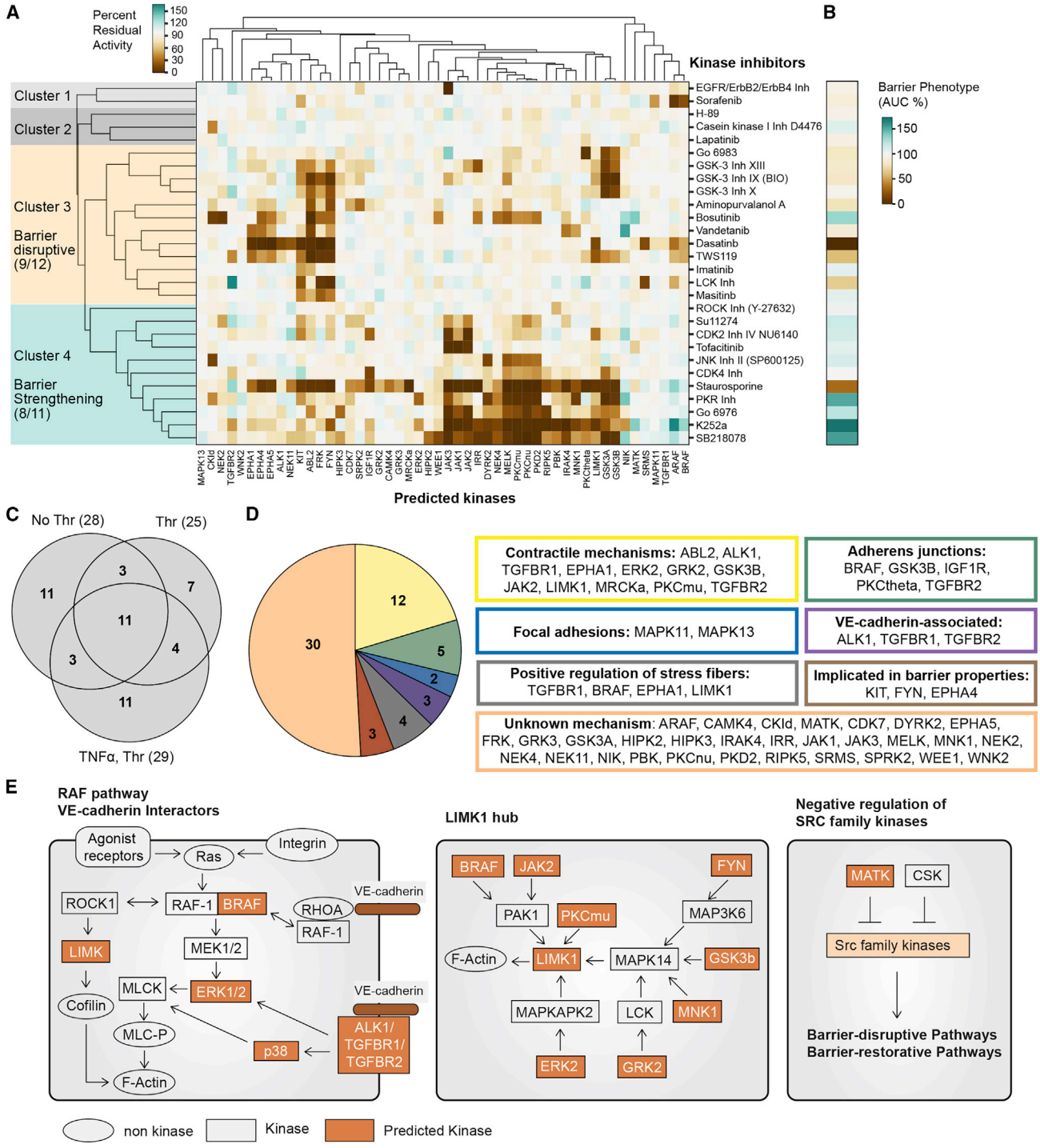

Figure 4. Kinase regression identifies kinases that are important in HBMEC barrier regulation

(A) Heatmap based on unsupervised hierarchical clustering of the residual activity of 50 predicted kinases targeted by the 28 kinase inhibitors used in HBMEC screens. Residual kinase activity data are from (Anastassiadis et al., 2011). Kinases were predicted by elastic net modeling based on kinase inhibitor screens in HBMECs under resting conditions and thrombin ± TNF-α activation. See also Data S1 and S2.

(B) Barrier phenotypes of the 28 kinase inhibitors based on the median AUC from screens of thrombin-activated HBMECs.

(C) Distribution of predicted kinases in each experimental condition.

(D) Pie chart showing predicted kinases not previously linked to barrier regulation (unknown mechanisms) as well as functional classification of predicted kinases implicated in barrier regulation. Some kinases fall into multiple categories. See also Table S2.

(E) Examples of pathways involved in barrier regulation with predicted kinases highlighted in orange. The LIMK1 hub was built based on PhosphoSitePlus v.6.5.9.3 (Hornbeck et al., 2012).

Please cite this article in press as: Dankwa et al., Exploiting polypharmacology to dissect host kinases and kinase inhibitors that modulate endothelial barrier integrity, Cell Chemical Biology (2021), https://doi.org/10.1016/j.chembiol.2021.06.004

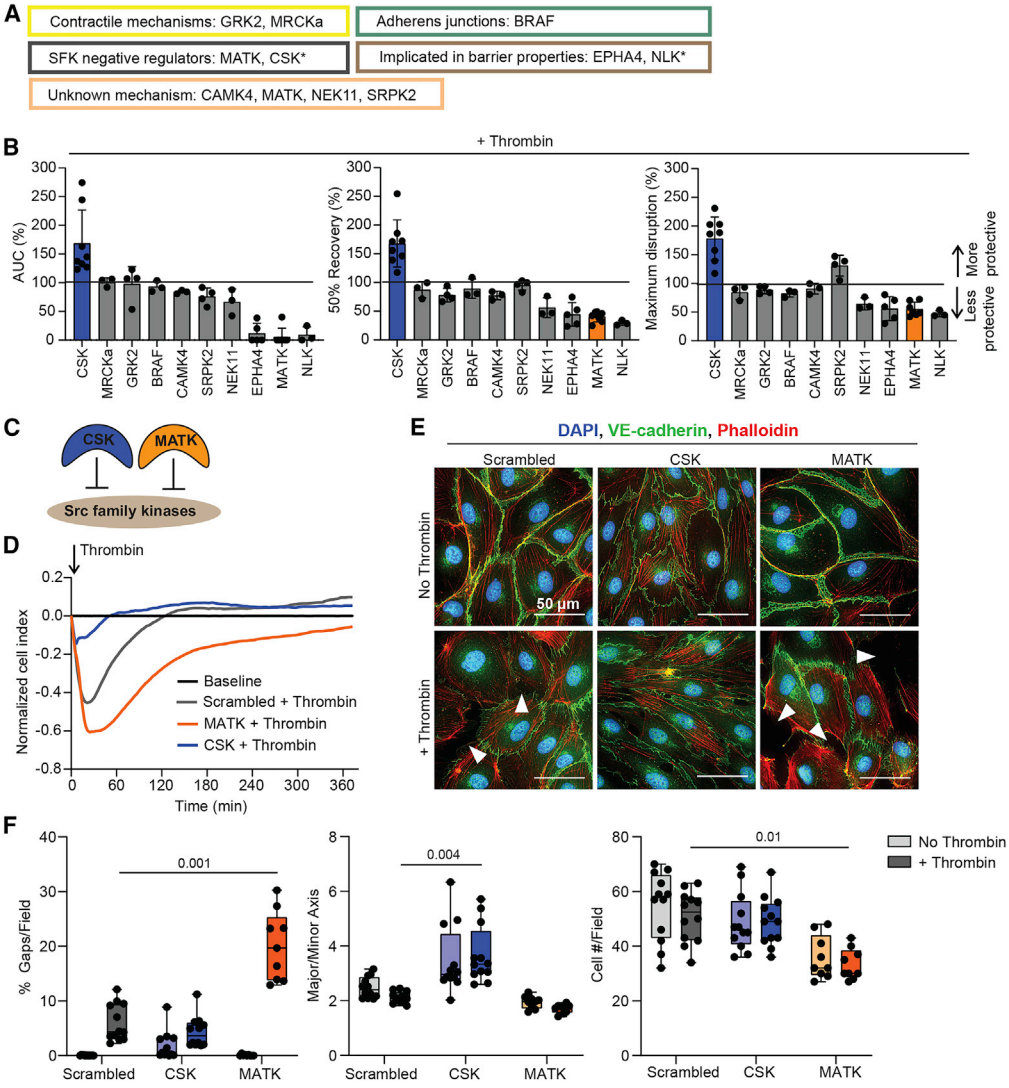

Figure 5. Multiple uncharacterized kinases contribute to endothelial barrier integrity

(A) Classification of kinases selected for shRNA knockdown. *CSK and NLK were not predicted by the KiR model.

(B) Effect of kinase knockdown on thrombin-treated HBMECs as determined by xCELLigence assays and represented as AUC, 50% recovery and maximum disruption. Scrambled control is set to 100%. Data are represented as mean ± SD of three to eight independent experiments, each in triplicate. See also Figures S3 and S4.

(C) CSK and MATK are negative regulators of Src family kinases.

(D) Recordings from an xCELLigence assay showing thrombin-treated CSK knockdown, MATK knockdown, and scrambled control cells. Baseline is the respective cell line without thrombin treatment.

(E) Images of CSK knockdown, MATK knockdown, and scrambled control cells in the resting state or 40 min after addition of thrombin. Arrowheads highlight gaps. Scale bars: 50 µm. Images are representative of three to four independent experiments.

(F) Quantification of images of thrombin-treated HBMECs at 40 min after addition of thrombin. Three fields were analyzed per experimental condition in each of three to four independent experiments. Black circles represent each field. Box and whisker plots show the median, 25th and 75th percentiles. Statistical significance between scrambled and knockdown cells in the presence or absence of thrombin was evaluated using Kruskal-Wallis and Dunn's multiple comparison tests.

Lentiviral-mediated shRNA knockdown of ten kinases decreased mRNA expression to levels ranging from undetected (MATK) to 40.0% ± 15.3% (BRAF), relative to expression of kinases in a non-targeting scrambled shRNA control (Figure S3A; Table S4). ARAF knockdown cells were not viable, so we could not investigate its role in endothelial barrier regulation using this approach.

Under resting conditions, knockdowns of GRK2, CAMK4, SRPK2, EPHA4, NLK, and CSK had a lower cell index by xCELLigence compared with the scrambled control (Figure S3B). By microscopy, GRK2, CAMK4, and CSK knockdown cells formed a mostly confluent monolayer with very small gaps, while SRPK2, EPHA4, and NLK knockdowns had larger gaps per field ($p < 0.0001$; Figures S3C and S3D), suggesting a role for these

Please cite this article in press as: Dankwa et al., Exploiting polypharmacology to dissect host kinases and kinase inhibitors that modulate endothelial barrier integrity, Cell Chemical Biology (2021), https://doi.org/10.1016/j.chembiol.2021.06.004

six kinases in endothelial barrier integrity. To assess the effect of kinase knockdown on cellular morphology, we measured the cell aspect ratio. Knockdown of CAMK4, SRPK2, and CSK resulted in more elongated or spindle-shaped cells, while MATK knockdown cells were larger and wider than the scrambled control cells (Figure S3C and S3D), suggesting these kinases play a role in regulating cell shape.

Next, xCELLigence assays were performed to study the effect of kinase knockdown on the thrombin response. To account for baseline differences in knockdown HBMECs relative to the scrambled control (Figure S3B), we set the resting state of each knockdown cell line as the baseline for the response of that cell line to thrombin, and then determined the AUC, recovery to baseline, and the cell index at maximal disruption (Figure S4A). By all three metrics, EPHA4, NLK, NEK11, and MATK knockdowns exacerbated thrombin-induced barrier disruption, whereas CSK knockdown substantially attenuated the effect of thrombin (Figure 5B). The only other kinase knockdown that blunted thrombin-induced barrier disruption was SRPK2, although the cells did not fully return to baseline (Figures 5B and S4A). The remaining knockdowns of BRAF, MRCKa, GRK2, and CAMK4 did not significantly alter thrombin's effect (Figures 5B and S4A). These findings by xCELLigence were consistent with microscopic examination of gap formation in thrombin-treated cells (Figure S4C).

Notably, knockdown of the two negative regulators of the SFKs (CSK and MATK) had opposing effects in the response of HBMECs to thrombin (Figures 5B–5D). The presence of modest gaps in the resting state in CSK knockdown cells (Figures 5E and 5F) makes protection against thrombin-induced barrier disruption even more striking. To investigate the opposing activities of CSK and MATK, we monitored VE-cadherin and actin remodeling by microscopy. Under resting conditions, CSK knockdown cells displayed a waviness in VE-cadherin staining, while MATK knockdown cells had a thicker, reticulated phenotype (Figure 5E). Under thrombin treatment, MATK knockdown cells had slower recovery of VE-cadherin at the cell periphery, compared with the scrambled control and CSK knockdown cells, which retained the wavy VE-cadherin pattern (Figure 5E). In addition, CSK did not prevent thrombin-induced actin stress fiber formation, even though there were fewer thrombin-induced gaps at 40 min (Figures 5E and 5F). Overall, the CSK and MATK knockdowns had distinct cellular phenotypes, despite both being negative regulators of the SFKs.

CSK and MATK knockdowns have distinct effects on the acute and sustained barrier-strengthening activity of kinase inhibitors

The four protective kinase inhibitors, K252a, bosutinib, PKR inhibitor, and SB 218078, affect many kinase targets and consequently, phosphosignaling networks. They also act with different temporal dynamics, conferring acute, delayed, or sustained barrier-strengthening activity. To investigate their barrier-strengthening activity, we explored how perturbation of the cellular state alters their activity. To this end, we knocked down CSK and MATK in HBMECs and assessed the temporal activity of K252a, bosutinib, PKR inhibitor, and SB 218078 on knockdown cells under resting conditions. Whereas MATK knockdown highly attenuated the early barrier-strengthening activity of bosutinib, it had little or no effect on the early activity of K252a and PKR inhibitor, or the slightly delayed activity of SB 218078 (Figures 6A, 6B, and S5). Conversely, CSK knockdown attenuated the early barrier-strengthening activity of PKR inhibitor and truncated the early activity of K252a but had limited effect on bosutinib. Furthermore, CSK knockdown largely abolished the sustained barrier-strengthening activity of K252a, PKR inhibitor, and SB 218078 (Figures 6A, 6B, and S5). MATK knockdown similarly abolished to a large extent the sustained barrier-strengthening activity of PKR inhibitor but only partially attenuated the late barrier-strengthening activity of K252a and SB 218078 (Figures 6A, 6B, and S5). Together, these findings suggest that MATK and CSK signaling pathways make distinct kinetic contributions to the activity of the four barrier-protective kinase inhibitors. They further highlight the disparate mechanisms of barrier strengthening of each of the four protective kinase inhibitors.

DISCUSSION

Efforts to understand the mechanisms that regulate endothelial permeability have revealed the centrality of phosphosignaling to this process. Nevertheless, we still lack a complete understanding of barrier maintenance and of how to translate our knowledge into effective barrier-restorative therapies. Here, we used a KiR approach to investigate kinase regulation of barrier function and to identify kinase inhibitors that can modulate endothelial barrier integrity. In doing so, we took advantage of polypharmacology to survey a significant portion of the human kinome, enabling a systems-level analysis of endothelial barrier regulation.

The KiR machine learning model predicted 50 kinases in the regulation of brain endothelial barrier integrity under resting and inflammatory conditions, of which 40% of the predicted kinases are known to play a role in endothelial barrier regulation, providing independent validation of the KiR approach. Of the predicted kinases not previously associated with barrier regulation, we demonstrated that NEK11, SRPK2, NLK, and MATK alter thrombin-induced barrier disruption, functionally linking these kinases to endothelial barrier regulation. For other kinases, such as EPHA4, known to be involved in barrier regulation but for which functional characterization is limited, we confirmed a role in barrier function and specifically demonstrated their involvement in the response to thrombin in endothelial cells.

Our study provides evidence that cells depleted of CSK and MATK, the two negative regulators of the SFKs, have contrasting responses to thrombin-induced barrier disruption and differentially alter the activities of four barrier-strengthening kinase inhibitors. The lack of a simple dichotomy between the roles of CSK and MATK in the early and late phases of activity of four barrier-protective kinase inhibitors further emphasizes the complex relationship between kinase targets and the signaling cascades they propagate. SFKs are known to contribute to both barrier disruption and barrier strengthening (Birukova et al., 2013; Han et al., 2013; Klomp et al., 2019; Knezevic et al., 2009; Mehta and Malik, 2006; Vouret-Craviari et al., 2002). Thus, one possibility is that CSK and MATK regulate different SFK members, which differentially influences barrier-disruptive and barrier-strengthening signaling. Alternatively, they may have SFK-independent

Please cite this article in press as: Dankwa et al., Exploiting polypharmacology to dissect host kinases and kinase inhibitors that modulate endothelial barrier integrity, Cell Chemical Biology (2021), https://doi.org/10.1016/j.chembiol.2021.06.004

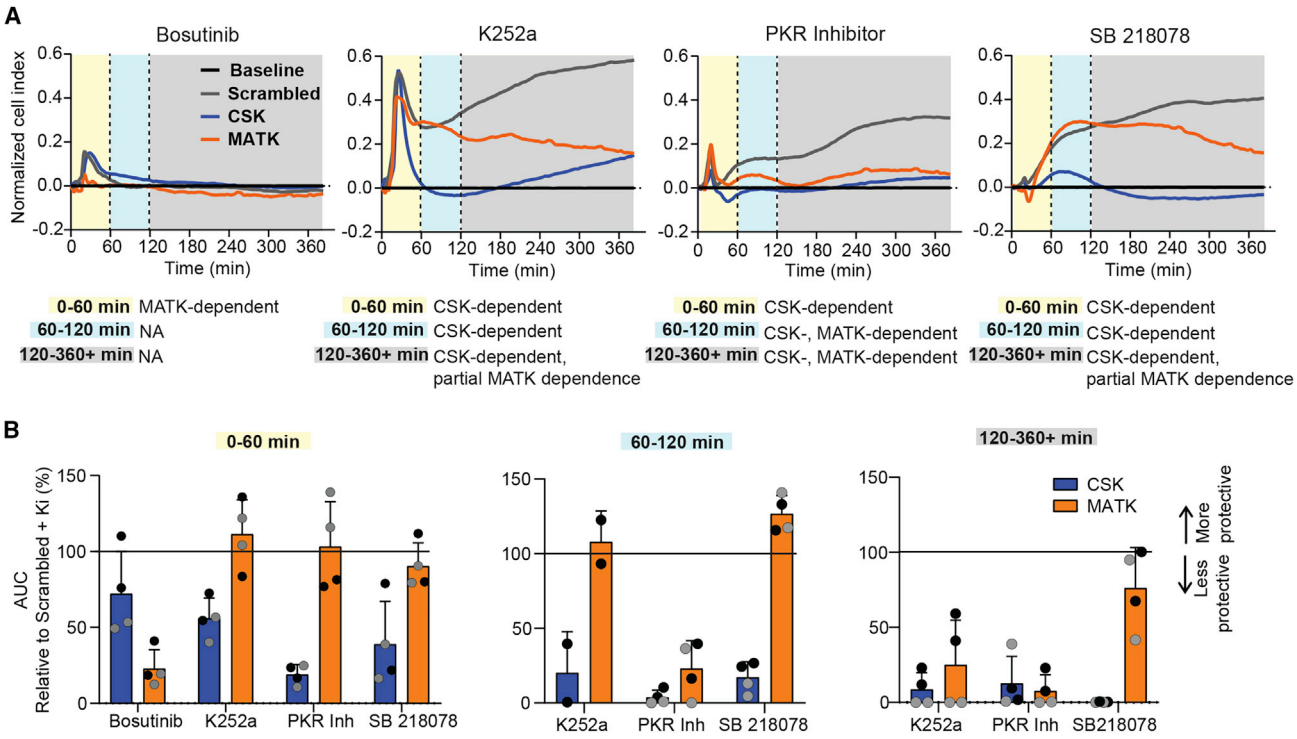

Figure 6. The SFK negative regulators CSK and MATK knockdowns have distinct effects on the acute and sustained barrier-strengthening activity of kinase inhibitors

(A) Phenotypes of CSK knockdown, MATK knockdown, and scrambled control HBMECs treated with 0.5 μM kinase inhibitors or DMSO. Shown are xCELLigence traces from one of four independent experiments. Baseline is each respective cell type + DMSO. CSK and MATK dependence during early and late phases of barrier strengthening are indicated.

(B) Temporal effect of protective kinase inhibitors on barrier properties of CSK knockdown and MATK knockdown cells, relative to the scrambled control. Data are represented as mean AUC ± SD of four independent experiments, each in triplicate. Negative cell index values were considered to be zero when determining the AUC. The scrambled control + each kinase inhibitor is set to 100%. Within the 60–120 min time period (middle graph) where the scrambled control + K252a had negative cell index values for biological replicates three and four, they were omitted from AUC analysis. Gray circles represent biological replicates three and four.

See also Figure S5.

roles. Indeed, CSK and MATK bind to different sets of phosphotyrosine-containing proteins via their Src homology 2 domain, which may facilitate recruitment to different cellular locations, thereby allowing for the distinct modulation of the activity of CSK and MATK (Ayrapetov et al., 2005).

BCR-ABL drugs have emerged as potential modulators of vascular permeability (Aman et al., 2012; Botros et al., 2020; Rizzo et al., 2015). However, the pleiotropic effect of kinase inhibitors on multiple kinase targets makes it challenging to disentangle their mechanism of action. Consistent with previous findings, ABL2 was one of the 50 kinases predicted by KiR to regulate barrier properties. However, our analysis suggests that ABL2 and MAP4K4 are insufficient to fully explain barrier phenotypes, suggesting that off-targets play an important role in the barrier-neutral (imatinib), barrier-strengthening (bosutinib), and barrier-disruptive (dasatinib) activity. The fact that all three BCR-ABL drugs target multiple, non-overlapping kinases that are known to play a role in barrier regulation (Anastassiadis et al., 2011; Haguet et al., 2018) likely explains their different barrier activities and may contribute to their distinct safety profiles. Whereas imatinib has minimal side effects, long-term use of dasatinib is sometimes associated with pleural effusion (Masiello et al., 2009) and thrombosis (Haguet et al., 2018). Dasatinib not only disrupted the endothelial barrier, but also exacerbated thrombin-induced barrier disruption, raising the possibility that there may be adverse interactions between dasatinib and inflammatory processes. Our screen also identified other kinase inhibitors that promote barrier strengthening, including K252a, PKR inhibitor, and SB 218078. The divergent polypharmacology they exhibit (Anastassiadis et al., 2011) likely contributes to their varying temporal activities for barrier strengthening and protection. Overall, our findings suggest that single classes of drugs may not have equal beneficial effect and that polypharmacology may modify the barrier activity of compounds.

This study has potential limitations. First, the KiR model is built on data where kinase inhibitors were assayed at 0.5 μM against 300 recombinant human kinases (Anastassiadis et al., 2011) and KiR is susceptible to false-negative and false-positive assignments (Gujral et al., 2014). It remains to be determined how differing concentrations may influence barrier phenotypes and the prediction of informative kinases. In addition, endothelial cell monolayer assays do not fully replicate the complexity of

microvasculature *in vivo* but, encouragingly, two of the barrier-protective kinase inhibitors that we identified have previously been shown to be protective in animal models of disease. PKR inhibitor has been shown to be neuroprotective in a neonatal rat model of hypoxia-ischemia injury (Xiao et al., 2016), while bosutinib attenuates vascular leak in mouse models of acute lung injury (Botros et al., 2020) and intracerebral hemorrhage, respectively (Ma et al., 2017). Finally, it is also possible that kinase inhibitors, such as imatinib, may be protective *in vivo*, even though they have limited barrier-strengthening activity *in vitro* potentially due to the experimental conditions used *in vitro*. In summary, our study supports the potential of BCR-ABL drugs and other kinase inhibitors as therapeutic modulators of endothelial barrier integrity and highlight the importance of polypharmacology in the mechanism of drug activity.

SIGNIFICANCE

Vascular leak is a pathological feature of a range of devastating conditions, including cerebral malaria and sepsis. Yet, there are limited strategies to repair and stabilize the endothelial barrier under inflammatory conditions. Drug repurposing of kinase inhibitors holds therapeutic promise because of the critical role of phosphosignaling in endothelial barrier regulation, but most kinase inhibitors lack selectivity, a feature termed polypharmacology. In this study, we used a systems-based, kinase regression (KiR) approach to study kinase regulation of the endothelial barrier and to explore how polypharmacology influences the barrier activity of kinase inhibitors. We demonstrated that three clinical BCR-ABL drugs have distinct barrier phenotypes attributable to their divergent combinatorial action on multiple kinases. Machine learning analysis predicted 50 kinases as being important in endothelial barrier regulation, including many previously uncharacterized kinases. We validated a role for multiple kinases in modifying the effect of thrombin on the endothelial barrier and observed opposing phenotypes of two negative regulators of SRC family kinases. Our work highlights the importance of polypharmacology in both the barrier activity of kinase inhibitors and how they interact with thrombin, a clotting factor implicated in vascular leak syndromes. These findings provide mechanistic insights into endothelial barrier regulation and have significant implications for the use of kinase inhibitors to therapeutically modulate endothelial barrier integrity in disease.

STAR★METHODS

Detailed methods are provided in the online version of this paper and include the following:

SUPPLEMENTAL INFORMATION

Supplemental information can be found online at https://doi.org/10.1016/j.chembiol.2021.06.004.

ACKNOWLEDGMENTS

This work was funded by the American Heart Association Postdoctoral Fellowship 19POST34390005 (to S.D.), National Institutes of Health (NIH) Training Grant T32 AI07509 (to E.K.K.G.), and NIH grant R01 HL130488 and R01 AI141602 (to A.K. and J.D.S).

AUTHOR CONTRIBUTIONS

S.D., A.K., and J.D.S. conceived and designed the experiments. S.D. and M.-M.D. performed the experiments. L.W. performed the KiR analyses. A.K. and J.D.S. jointly supervised the project. S.D., A.K., and J.D.S. wrote the paper with input from all co-authors. All authors approved the final version of the manuscript.

DECLARATION OF INTERESTS

The authors declare no competing interests.

INCLUSION AND DIVERSITY

One or more of the authors of this paper self-identifies as an underrepresented ethnic minority in science.

Received: December 18, 2020
Revised: April 29, 2021
Accepted: June 9, 2021
Published: July 2, 2021

REFERENCES

Aird, W.C. (2007). Phenotypic heterogeneity of the endothelium: I. Structure, function, and mechanisms. Circ Res. *100*, 158–173.

Aman, J., van Bezu, J., Damanafshan, A., Huveneers, S., Eringa, E.C., Vogel, S.M., Groeneveld, A.B., Vonk Noordegraaf, A., van Hinsbergh, V.W., and van Nieuw Amerongen, G.P. (2012). Effective treatment of edema and endothelial barrier dysfunction with imatinib. Circulation *126*, 2728–2738.

Anastassiadis, T., Deacon, S.W., Devarajan, K., Ma, H., and Peterson, J.R. (2011). Comprehensive assay of kinase catalytic activity reveals features of kinase inhibitor selectivity. Nat. Biotechnol. *29*, 1039–1045.

Arang, N., Kain, H.S., Glennon, E.K., Bello, T., Dudgeon, D.R., Walter, E.N.F., Gujral, T.S., and Kaushansky, A. (2017). Identifying host regulators and inhibitors of liver stage malaria infection using kinase activity profiles. Nat. Commun. *8*, 1232.

Ayrapetov, M.K., Nam, N.H., Ye, G., Kumar, A., Parang, K., and Sun, G. (2005). Functional diversity of Csk, Chk, and Src SH2 domains due to a single residue variation. J. Biol. Chem. *280*, 25780–25787.

Birukova, A.A., Tian, X., Tian, Y., Higginbotham, K., and Birukov, K.G. (2013). Rap-afadin axis in control of Rho signaling and endothelial barrier recovery. Mol. Biol. Cell *24*, 2678–2688.

Botros, L., Pronk, M.C.A., Juschten, J., Liddle, J., Morsing, S.K.H., van Buul, J.D., Bates, R.H., Tuinman, P.R., van Bezu, J.S.M., Huveneers, S., et al. (2020). Bosutinib prevents vascular leakage by reducing focal adhesion turnover and reinforcing junctional integrity. J. Cell Sci. *133*, jcs240077.

Chang, R., Cardenas, J.C., Wade, C.E., and Holcomb, J.B. (2016). Advances in the understanding of trauma-induced coagulopathy. Blood *128*, 1043–1049.

Chong, Y.P., Mulhern, T.D., and Cheng, H.C. (2005). C-terminal Src kinase (CSK) and CSK-homologous kinase (CHK)—endogenous negative regulators of Src-family protein kinases. Growth Factors *23*, 233–244.

Dorard, C., Cseh, B., Ehrenreiter, K., Wimmer, R., Varga, A., Hirschmugl, T., Maier, B., Kramer, K., Furlinger, S., Doma, E., et al. (2019). RAF dimers control vascular permeability and cytoskeletal rearrangements at endothelial cell-cell junctions. FEBS J. *286*, 2277–2294.

Erice, C., and Kain, K.C. (2019). New insights into microvascular injury to inform enhanced diagnostics and therapeutics for severe malaria. Virulence *10*, 1034–1046.

Fazakas, C., Nagaraj, C., Zabini, D., Vegh, A.G., Marsh, L.M., Wilhelm, I., Krizbai, I.A., Olschewski, H., Olschewski, A., and Balint, Z. (2018). Rho-kinase inhibition ameliorates dasatinib-induced endothelial dysfunction and pulmonary hypertension. Front. Physiol. *9*, 537.

Gallego-Delgado, J., Basu-Roy, U., Ty, M., Alique, M., Fernandez-Arias, C., Movila, A., Gomes, P., Weinstock, A., Xu, W., Edagha, I., et al. (2016). Angiotensin receptors and beta-catenin regulate brain endothelial integrity in malaria. J. Clin. Invest. *126*, 4016–4029.

Garcia, J.G., Liu, F., Verin, A.D., Birukova, A., Dechert, M.A., Gerthoffer, W.T., Bamberg, J.R., and English, D. (2001). Sphingosine 1-phosphate promotes endothelial cell barrier integrity by Edg-dependent cytoskeletal rearrangement. J. Clin. Invest. *108*, 689–701.

Giannotta, M., Trani, M., and Dejana, E. (2013). VE-cadherin and endothelial adherens junctions: active guardians of vascular integrity. Dev. Cell *26*, 441–454.

Glennon, E.K.K., Dankwa, S., Smith, J.D., and Kaushansky, A. (2018). Opportunities for host-targeted therapies for malaria. Trends Parasitol. *34*, 843–860.

Gujral, T.S., Peshkin, L., and Kirschner, M.W. (2014). Exploiting polypharmacology for drug target deconvolution. Proc. Natl. Acad. Sci. U S A *111*, 5048–5053.

Haguet, H., Douxfils, J., Chatelain, C., Graux, C., Mullier, F., and Dogne, J.M. (2018). BCR-ABL tyrosine kinase inhibitors: which mechanism(s) may explain the risk of thrombosis? TH Open *2*, e68–e88.

Han, J., Zhang, G., Welch, E.J., Liang, Y., Fu, J., Vogel, S.M., Lowell, C.A., Du, X., Cheresh, D.A., Malik, A.B., et al. (2013). A critical role for Lyn kinase in strengthening endothelial integrity and barrier function. Blood *122*, 4140–4149.

Hornbeck, P.V., Kornhauser, J.M., Tkachev, S., Zhang, B., Skrzypek, E., Murray, B., Latham, V., and Sullivan, M. (2012). PhosphoSitePlus: a comprehensive resource for investigating the structure and function of experimentally determined post-translational modifications in man and mouse. Nucleic Acids Res. *40*, D261–D270.

Janes, K.A., Albeck, J.G., Gaudet, S., Sorger, P.K., Lauffenburger, D.A., and Yaffe, M.B. (2005). A systems model of signaling identifies a molecular basis set for cytokine-induced apoptosis. Science *310*, 1646–1653.

Klaeger, S., Heinzlmeir, S., Wilhelm, M., Polzer, H., Vick, B., Koenig, P.A., Reinecke, M., Ruprecht, B., Petzoldt, S., Meng, C., et al. (2017). The target landscape of clinical kinase drugs. Science *358*, eaan4368.

Klomp, J.E., Shaaya, M., Matsche, J., Rebiai, R., Aaron, J.S., Collins, K.B., Huyot, V., Gonzalez, A.M., Muller, W.A., Chew, T.L., et al. (2019). Time-variant SRC kinase activation determines endothelial permeability response. Cell Chem. Biol. *26*, 1081–1094.e6.

Knezevic, N., Tauseef, M., Thennes, T., and Mehta, D. (2009). The G protein betagamma subunit mediates reannealing of adherens junctions to reverse endothelial permeability increase by thrombin. J. Exp. Med. *206*, 2761–2777.

Komarova, Y.A., Kruse, K., Mehta, D., and Malik, A.B. (2017). Protein interactions at endothelial junctions and signaling mechanisms regulating endothelial permeability. Circ. Res. *120*, 179–206.

Komarova, Y.A., Mehta, D., and Malik, A.B. (2007). Dual regulation of endothelial junctional permeability. Sci. STKE *2007*, re8.

Kuppers, V., Vockel, M., Nottebaum, A.F., and Vestweber, D. (2014). Phosphatases and kinases as regulators of the endothelial barrier function. Cell Tissue Res. *355*, 577–586.

Levi, M., and van der Poll, T. (2010). Inflammation and coagulation. Crit. Care Med. *38*, S26–S34.

Levi, M., and van der Poll, T. (2017). Coagulation and sepsis. Thromb. Res. *149*, 38–44.

Ma, L., Manaenko, A., Ou, Y.B., Shao, A.W., Yang, S.X., and Zhang, J.H. (2017). Bosutinib attenuates inflammation via inhibiting salt-inducible kinases in experimental model of intracerebral hemorrhage on mice. Stroke *48*, 3108–3116.

Masiello, D., Gorospe, G., 3rd, and Yang, A.S. (2009). The occurrence and management of fluid retention associated with TKI therapy in CML, with a focus on dasatinib. J. Hematol. Oncol. *2*, 46.

McVerry, B.J., and Garcia, J.G. (2004). Endothelial cell barrier regulation by sphingosine 1-phosphate. J. Cell Biochem. *92*, 1075–1085.

Mehta, D., and Malik, A.B. (2006). Signaling mechanisms regulating endothelial permeability. Physiol. Rev. *86*, 279–367.

Moxon, C.A., Wassmer, S.C., Milner, D.A., Jr., Chisala, N.V., Taylor, T.E., Seydel, K.B., Molyneux, M.E., Faragher, B., Esmon, C.T., Downey, C., et al. (2013). Loss of endothelial protein C receptors links coagulation and inflammation to parasite sequestration in cerebral malaria in African children. Blood *122*, 842–851.

Okada, M. (2012). Regulation of the SRC family kinases by Csk. Int. J. Biol. Sci. *8*, 1385–1397.

Orsenigo, F., Giampietro, C., Ferrari, A., Corada, M., Galaup, A., Sigismund, S., Ristagno, G., Maddaluno, L., Koh, G.Y., Franco, D., et al. (2012). Phosphorylation of VE-cadherin is modulated by haemodynamic forces and contributes to the regulation of vascular permeability in vivo. Nat. Commun. *3*, 1208.

Park-Windhol, C., and D'Amore, P.A. (2016). Disorders of vascular permeability. Annu. Rev. Pathol. *11*, 251–281.

Pober, J.S., and Sessa, W.C. (2007). Evolving functions of endothelial cells in inflammation. Nat. Rev. Immunol. *7*, 803–815.

Pober, J.S., and Sessa, W.C. (2015). Inflammation and the blood microvascular system. Cold Spring Harb Perspect. Biol. *7*, a016345.

Radeva, M.Y., and Waschke, J. (2018). Mind the gap: mechanisms regulating the endothelial barrier. Acta Physiol. (Oxf) *222*. https://doi.org/10.1111/apha.12860.

Reddy, A.S., and Zhang, S. (2013). Polypharmacology: drug discovery for the future. Expert Rev. Clin. Pharmacol. *6*, 41–47.

Rizzo, A.N., Aman, J., van Nieuw Amerongen, G.P., and Dudek, S.M. (2015). Targeting Abl kinases to regulate vascular leak during sepsis and acute respiratory distress syndrome. Arterioscler Thromb. Vasc. Biol. *35*, 1071–1079.

Roskoski, R., Jr. (2021). Properties of FDA-approved small molecule protein kinase inhibitors: a 2021 update. Pharmacol. Res. *165*, 105463.

Schneider, C.A., Rasband, W.S., and Eliceiri, K.W. (2012). NIH Image to ImageJ: 25 years of image analysis. Nat. Methods *9*, 671–675.

van den Biggelaar, M., Hernandez-Fernaud, J.R., van den Eshof, B.L., Neilson, L.J., Meijer, A.B., Mertens, K., and Zanivan, S. (2014). Quantitative phosphoproteomics unveils temporal dynamics of thrombin signaling in human endothelial cells. Blood *123*, e22–36.

Vouret-Craviari, V., Bourcier, C., Boulter, E., and van Obberghen-Schilling, E. (2002). Distinct signals via Rho GTPases and Src drive shape changes by

thrombin and sphingosine-1-phosphate in endothelial cells. J. Cell Sci. *115*, 2475–2484.

Wallez, Y., Cand, F., Cruzalegui, F., Wernstedt, C., Souchelnytskyi, S., Vilgrain, I., and Huber, P. (2007). Src kinase phosphorylates vascular endothelial-cadherin in response to vascular endothelial growth factor: identification of tyrosine 685 as the unique target site. Oncogene *26*, 1067–1077.

Woodruff, T.M., Wu, M.C., Morgan, M., Bain, N.T., Jeanes, A., Lipman, J., Ting, M.J., Boyd, A.W., Taylor, S.M., and Coulthard, M.G. (2016). Epha4-Fc treatment reduces ischemia/reperfusion-induced intestinal injury by inhibiting vascular permeability. Shock *45*, 184–191.

Xiao, J., Tan, Y., Li, Y., and Luo, Y. (2016). The specific protein kinase R (PKR) inhibitor C16 protects neonatal hypoxia-ischemia brain damages by inhibiting neuroinflammation in a neonatal rat model. Med. Sci. Monit. *22*, 5074–5081.

Yuan, S.Y. (2002). Protein kinase signaling in the modulation of microvascular permeability. Vascul. Pharmacol. *39*, 213–223.

Please cite this article in press as: Dankwa et al., Exploiting polypharmacology to dissect host kinases and kinase inhibitors that modulate endothelial barrier integrity, Cell Chemical Biology (2021), https://doi.org/10.1016/j.chembiol.2021.06.004

STAR★METHODS

KEY RESOURCES TABLE

REAGENT or RESOURCE	SOURCE	IDENTIFIER
Antibodies		
Rabbit polyclonal anti-VE-cadherin	Abcam	Cat#ab33168; RRID: AB_870662
Goat anti-rabbit IgG secondary antibody Alexa fluor 488	Thermo Fisher Scientific	Cat#A-11008; RRID: AB_143165
Chemicals, Peptides, and Recombinant Proteins		
Kinase inhibitors; see Table S1	Selleck Chemicals	See Table S1
Thrombin from human plasma	Sigma-Aldrich	Cat#T6884; CAS 9002-04-4
Tumor necrosis factor alpha (TNFα)	Sigma-Aldrich	Cat#T0157
Experimental Models: Cell Lines		
Human: Primary HBMECs	Cell Systems	Cat#ACBRI 376
Human: Primary HUVECs	Lonza	Cat#CC-2519
Oligonucleotides		
qPCR primers for human kinases and controls; see Table S4	https://pga.mgh.harvard.edu/primerbank/	See Table S4
Recombinant DNA		
MISSION® shRNA human kinase vectors; see Table S3	Sigma-Aldrich	See Table S3
Software and Algorithms		
Seaborn (Python 3.7.6)	https://seaborn.pydata.org/	https://github.com/mwaskom/seaborn
Glmnet (Python 3.7.6)	https://web.stanford.edu/~hastie/glmnet_python/	https://github.com/bbalasub1/glmnet_python
PhosphoSitePlus v6.5.9.3	Hornbeck et al., 2012	https://www.phosphosite.org/homeAction.action
ImageJ	Schneider et al., 2012	https://imagej.nih.gov/ij/
Other		
Alexa Fluor 647 Phalloidin	Thermo Fisher Scientific	Cat#A22287; RRID:AB_2620155

RESOURCE AVAILABILITY

Lead contact

Further information and requests for resources and reagents should be directed to and will be fulfilled by the Lead Contact, Joseph D. Smith (joe.smith@seattlechildrens.org).

Materials availability

This study did not generate new unique reagents.

Data and code availability

This manuscript includes all kinase inhibitor screen datasets (Data S1) and Kinase Regression code (Data S2) generated or analyzed during this study.

EXPERIMENTAL MODEL AND SUBJECT DETAILS

Cell lines

Primary HBMECs (Cell Systems Cat# ACBRI 376) were maintained on attachment factor (Cell Systems Cat# 4Z0-201) or 4-5 μg/cm^2 collagen (Corning Cat# 354236) in HBMEC culture media (Lonza Cat# CC-3202 or PromoCell Cat# C-22121) at 37°C and 5% CO_2. HBMECs were used until passage 10. Primary HUVECs (Lonza Cat# CC-2519) were cultured on attachment factor or 4-5 μg/cm^2 collagen in HUVEC culture media (Lonza Cat# CC-3124 or PromoCell Cat# C-22120) at 37°C and 5% CO_2. HUVECs were used until passage 9. We do not have access to gender information on the commercially purchased primary endothelial cells. HEK293-FT cells (Arang et al., 2017) were maintained in DMEM (Corning) supplemented with 10% FBS, 10 mM HEPES, 6 mM L-glutamine, 2 mM

Please cite this article in press as: Dankwa et al., Exploiting polypharmacology to dissect host kinases and kinase inhibitors that modulate endothelial barrier integrity, Cell Chemical Biology (2021), https://doi.org/10.1016/j.chembiol.2021.06.004

sodium pyruvate (Gibco), 1x non-essential amino acids (Gibco), 2.5% penicillin/streptomycin (Gibco) and fungizone (HyClone) at 37°C and 5% CO_2.

METHOD DETAILS

Kinase inhibitor xCELLigence assays

xCELLigence plates were seeded with HBMECs or HUVECs at 10,000-12,000 cells/well and grown to confluency for 3-4 days during which time growth was monitored with cell index readings every 2-4 h. On the day of the assay, for the kinase inhibitor screen without thrombin, kinase inhibitors (Selleck Chemicals; Table S1) previously made up to 1 mM in DMSO were added to triplicate wells at a final concentration of 0.5 μM (dilutions in media without FBS; serum-free culture media). Recordings were taken every minute for 30 mins and then every 5 min for 1.5 h. A similar experimental setup was used for the dose titration (0.03 μM to 2 μM) of bosutinib, dasatinib and imatinib on resting cells. For the kinase inhibitor screen with thrombin, cells were equilibrated in serum-free culture media for 1-2 h, after which, thrombin (Sigma-Aldrich Cat# T6884; CAS 9002-04-4) was added to wells at a final concentration of 5 nM. Recordings were taken every minute for 6 mins, then kinase inhibitors were added to triplicate wells at a final concentration of 0.5 μM. The cell index was measured every minute for 2 h and then every 5 min for 4 h. A similar experimental setup was used for the dose titration (0.13 μM to 2 μM) of bosutinib, dasatinib and imatinib on thrombin-treated cells. Conversely, for assays to determine how kinase inhibitors alter thrombin treatment, kinase inhibitors were added to HBMECs 15 min before addition of thrombin. Recordings were taken every minute during kinase inhibitor treatment and for the first 2 h of thrombin treatment, followed by recordings every 5 min for 4 h. The TNFα + thrombin + kinase inhibitor screen was performed identically to the thrombin + kinase inhibitor screen, except that HBMECs were activated with 10 ng/ml TNFα (Sigma-Aldrich Cat# T0157) for ~22 h before media equilibration on the day of the assay. Cells exposed to media only were set as the baseline in each instance. Control samples were cells treated with DMSO (assays of resting cells), thrombin + DMSO (assays of thrombin-activated cells) or TNFα + thrombin + DMSO (assays of TNFα + thrombin-activated cells).

Kinase regression

We applied the elastic net regularization approach for drug target deconvolution (Gujral et al., 2014), which, by reducing the dimension of a relatively large data space (i.e. 28 kinase inhibitors x 300 kinases), can robustly extract the most informative kinases involved in barrier regulation. Using the normalized AUC values from xCELLigence HBMEC kinase inhibitor screens as phenotypic readouts for barrier integrity (Data S1), along with the biochemical profiles of the kinase inhibitors against 300 recombinant protein kinases (Anastassiadis et al., 2011), the linear regression algorithm downselected a subset of 50 kinase targets that are more influential in driving the observed HBMEC barrier phenotypes. To enhance the performance of model selection, a condition-specific cross-validation strategy was used. Glmnet package in Python 3.7.6 (https://github.com/bbalasub1/glmnet_python) was used to fit the generalized linear models via penalized maximum likelihood, with the elastic net mixing parameter α of 0.8, which confers relative stringency. The regularization path was computed for elastic net penalty at a grid of values for the regularization parameter λ of 10^3. The kinases with non-zero coefficients were predicted to be informative for the measured barrier phenotypes. See also Data S2.

Apoptosis assays

HBMECs were seeded in 6-well plates at 80,000 cells/well and grown to confluency for 3 days. On the day of the assay, kinase inhibitors (Selleck Chemicals; Table S1) were added to wells at a final concentration of 0.5 μM for 6 h under culture conditions. Cells in suspension together with cells detached by trypsinization were then labeled with Annexin V-FITC and propidium iodide (PI) according to the manufacturer's protocol (Miltenyi Biotec Cat# 130-092-052). The relative Annexin V/PI fluorescence was measured by flow cytometry on an LSRII flow cytometer (BD Biosciences). Data were analyzed using FlowJo v10.5.3 (BD).

Preparation of lentivirus

10 cm^2 tissue culture-treated dishes were seeded with 3 x 10^6 HEK293-FT cells. The following day, cells were transfected at 70-80% confluency with 1.5 μg of pCMV-VSV-G envelope plasmid, 3 μg of psPax2 packaging plasmid and 6 μg of pLKO.1 plasmid harboring shRNA against a kinase of interest (MISSION shRNA vectors (Sigma-Aldrich; Table S3) or with a non-targeting scrambled shRNA (Sigma-Aldrich). 21 μl of 1 mg/ml polyethylenimine MAX (Polysciences Inc) was mixed with pCMV-VSV-G, psPax2, pLKO.1 in serum-free DMEM and incubated for 10 min. Transfection mixtures were added dropwise to HEK293-FT cells. Media was changed the following day. Culture supernatant containing lentiviral particles was harvested approximately 24 h after the media change and stored at -80°C until needed.

shRNA knockdown of host kinases

Lentivirus transduction of HBMECs for knockdown of host kinases was performed directly in the vessels in which the effect of the knockdown was to be measured and at the time of cell seeding. For immunofluorescence assays, collagen type I-coated chamber slides were seeded with HBMECs at 10,000 cells/well and with 125 μl lentivirus. For xCELLigence assays, plates were seeded with HBMECs at 6,000 cells/well and with 50 μl lentivirus. For measuring the extent of kinase knockdown, 6-well or 12-well plates were seeded with HBMECs at 80,000 cells/well or 40,000 cells/well and with 1000 μl or 500 μl lentivirus, respectively. HBMECs were transduced with 1 μg/ml polybrene. 24 h post-transduction, transductants were selected with 2 ug/ml puromycin. Cells were grown

Please cite this article in press as: Dankwa et al., Exploiting polypharmacology to dissect host kinases and kinase inhibitors that modulate endothelial barrier integrity, Cell Chemical Biology (2021), https://doi.org/10.1016/j.chembiol.2021.06.004

under puromycin selection for 2-3 days at which time cells in the 6-well or 12-well plates were harvested for RNA extraction and xCELLigence assays and immunofluorescence assays were performed.

qRT-PCR quantification of kinase expression

RNA was extracted from TRIzol (Thermo Fisher) homogenates by chloroform-based separation. Briefly, 0.2 ml chloroform was added for every 0.75 ml of TRIzol Reagent used. Samples were shaken vigorously, incubated at room temperature for 10 min and then centrifuged at 3000 RPM at 4°C for 30 min. RNA contained in the aqueous upper phase was purified using the RNeasy Mini kit (Qiagen) according to the manufacturer's protocol. cDNA was prepared from equal amounts of DNase-treated RNA of each sample using multi-scribe reverse transcriptase and random hexamers with incubation for 10 min at 25°C, 30 min at 48°C and 5 min at 95°C. qPCR was performed using Power SYBR Green PCR Master Mix (Applied Biosystems, Life Technologies) and host-specific primers (Primer Bank: https://pga.mgh.harvard.edu/primerbank/; Table S4). Samples were run on an Applied Biosystems 7500 with the following amplification conditions: 95°C for 10 min, 40 cycles of 95°C for 15 sec and 60°C for 1 min, followed by a melt curve stage. Relative transcript abundance was determined by normalization to the housekeeping gene, beta actin, followed by normalization to kinase expression in the scrambled control sample according to the $2^{-\Delta\Delta CT}$ method.

Immunofluorescence microscopy

Collagen type I-coated chamber slides (Corning BioCoat™) were seeded with HBMECs at 10,000 cells/well and grown to confluency. After treatment according to experimental conditions, the cells were fixed in 3.7% paraformaldehyde for 20 min and washed three times with PBS. The cells were then incubated in Background Buster (Innovex) for 30 min, followed by blocking buffer (2% bovine serum albumin (BSA), 0.1% Triton X-100 in PBS) for 1 h. Cells were incubated overnight with rabbit anti-VE-cadherin antibody (1:200, Abcam Cat# ab33168, RRID: AB_870662) and Alexa Fluor 647 phalloidin (1:50, Thermo Fisher Scientific Cat# A22287, RRID:AB_2620155) diluted in blocking buffer. After washing four times in PBS, cells were incubated in goat anti-rabbit Alexa Fluor 488 antibody (1:200, Thermo Fisher Scientific Cat# A-11008, RRID: AB_143165) and 8 μg/ml DAPI (Sigma Aldrich) diluted in PBS-2% BSA-5% goat serum. Cells were washed four times in PBS after which Prolong™ Gold antifade mounting medium (Thermo Fisher Scientific) was added. Images were acquired at 200x magnification using a Nikon Ti-E inverted fluorescence microscope at 1024 x 1280 pixels (328.73 x 410.91 μm) or at 400x magnification on a DeltaVision Elite Deconvolution microscope at 976 x 976 pixels (155.66 μm x 155.66 μm) and 15-25 Z stacks with a z-step distance of 0.1 μm.

Image analysis

All image analysis was done using ImageJ v1.50e (NIH; https://imagej.nih.gov/ij/) (Schneider et al., 2012). Three representative images acquired at 200x magnification on the Nikon Ti-E inverted fluorescence microscope were chosen from each condition for analysis. The cell number was recorded using the "cell counter" plugin. Gaps were defined as areas outside a cell lacking any VE-cadherin staining. Gaps were measured by increasing the brightness of the FITC channel and consequently, VE-cadherin staining, so that the contrast between each cell (the interior and boundaries) and the background was clear. The threshold tool, with default settings for a dark background, was used to highlight the zero-to-low intensity pixels outside the cells, until the gaps alone were completely selected (see Figure S4B). The aspect ratio was determined by using the line tool to measure the length of the long and short axis of each cell in the field. Across the three independent experiments for kinase inhibition assays, aspect ratio was determined for 204 to 376 cells, with a median cell number of 300. For kinase knockdown images, aspect ratio was determined for 121 to 484 cells, with a median cell number of 184. Final images presented here were edited using ImageJ by adjusting each color channel linearly using the "Brightness/Contrast" tool.

xCELLigence assays of kinase knockdowns

After HBMEC transductions, growth was monitored with readings every 1-2 h. On the day of the assay, cells were equilibrated in serum-free media for 1-2 h, and then thrombin or kinase inhibitors were added to triplicate wells at a final concentration of 5 nM (thrombin) or 0.5 μM (kinase inhibitors). Recordings were taken every minute for 2 h and then every 5 min for 4 h. Control wells for each kinase knockdown cell type received serum-free media and became the baseline against which the effect of thrombin or kinase inhibitors was measured.

Analysis of xCELLigence assays

For analysis of xCELLigence assays, the cell index was normalized to baseline at the timepoint just before addition of either kinase inhibitors or thrombin. AUC values were normalized by subtraction of the control AUC value and then linearly transformed. The most minimum normalized AUC value in a dataset for a single experiment was set to zero, while the normalized value for the control sample was set to 100%. For temporal analysis of kinase inhibitor screens, these fixed numbers were set for each time interval, making it possible to compare transformed AUC values within, but not across time intervals. For temporal analysis of kinase knockdown cells treated with barrier-strengthening kinase inhibitors, negative cell index values were considered as zero, and the resulting AUC was normalized to the AUC for control cells (scrambled + kinase inhibitor). In instances where the AUC of control cells was zero, the normalized AUC for experimental samples was undefined and thus omitted from further analysis. The 50% recovery cell index was defined as the cell index of thrombin + kinase inhibitor-treated cells or thrombin-treated kinase knockdown cells at the time point at which control cells have recovered by 50% (see Figure S2B). Maximum disruption was defined as the most negative cell index for

each sample in an assay. 50% recovery and maximum disruption values were transformed by subtraction of the cell index for control cells and exponentiation of this number to base 10.

QUANTIFICATION AND STATISTICAL ANALYSES

Statistical analyses were performed using GraphPad Prism version 8.1.0. Differences between the control and experimental groups were evaluated using Kruskal-Wallis non-parametric test followed by Dunn's multiple comparisons test for image analyses, and one-way ANOVA followed by Dunnett's multiple comparisons test for apoptosis assays. Statistical significance was considered as $P < 0.05$. Correlations between variables were assessed using Pearson correlation analysis. Heatmaps were generated using the statistical data visualization library seaborn in Python 3.7.6 (https://github.com/mwaskom/seaborn). Additional statistical details of experiments including biological and technical replicates, dispersion and precision measures are indicated in figure legends.

Cell Chemical Biology, Volume *28*

Supplemental information

Exploiting polypharmacology to dissect host kinases and kinase inhibitors that modulate endothelial barrier integrity

Selasi Dankwa, Mary-Margaret Dols, Ling Wei, Elizabeth K.K. Glennon, Heather S. Kain, Alexis Kaushansky, and Joseph D. Smith

SUPPLEMENTAL INFORMATION

Supplemental Items:

Supplemental Figures S1-S5

Tables S1, S3-S4

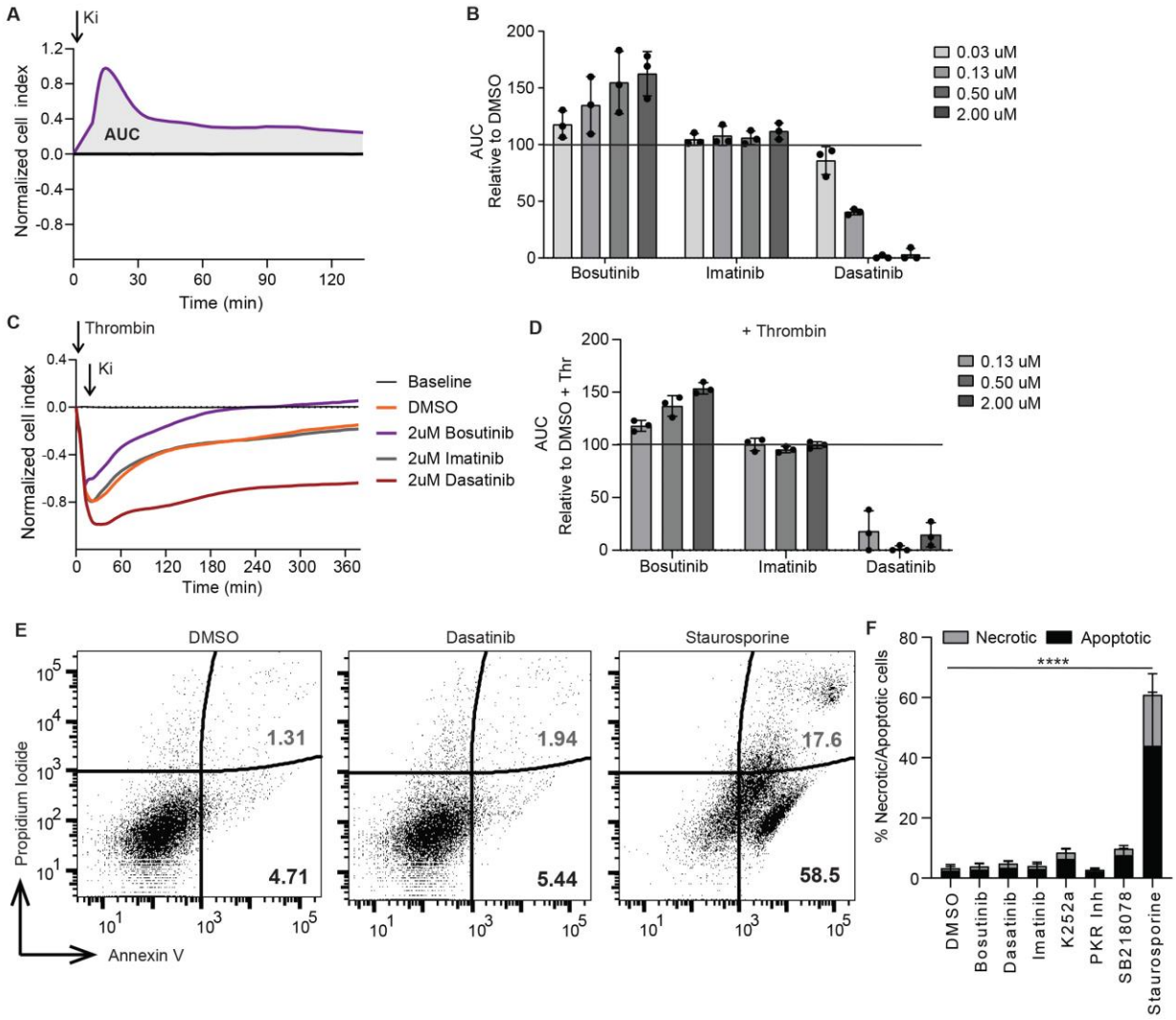

Figure S1. Dose-dependent effect of BCR-ABL kinase inhibitors on the HBMEC barrier and lack of effect on cell viability. Related to Figures 1 and 2.
(A) Recording from an xCELLigence assay illustrating area under the curve (AUC).

(B) Dose-dependent effect of bosutinib and dasatinib on the resting barrier as determined by the AUC.
(C) Representative recordings from an xCELLigence assay showing the normalized cell index after addition of 2 µM bosutinib, imatinib and dasatinib to HBMECs pre-treated with 5 nM thrombin. (See also Figure 1B).
(A, C) Ki: Kinase inhibitor
(D) Dose-dependent effect of bosutinib on thrombin-treated HBMECs as determined by the AUC. Note that there is a greater difference between the barrier-protective and -restorative effect of bosutinib and the neutral effect of imatinib at 2 µM compared to 0.5 µM.
(B, D) >100%: barrier-strengthening, <100%: barrier-disruption. Data are represented as mean ± SD of 3 independent experiments, each done in triplicate wells.
(E) Flow cytometry dot plots illustrating the percentage of apoptotic cells (bottom right quadrant) and necrotic cells (top right quadrant) after treating HBMECs with 0.5 µM dasatinib, staurosporine or DMSO for 6 h.
(F) Quantification from flow cytometry of the effect on cell viability after treatment of HBMECs with 0.5 µM of the indicated kinase inhibitors or DMSO for 6 h. Statistically significant comparisons with DMSO were determined by one-way ANOVA followed by Dunnett's multiple comparisons test. ****$P < 0.0001$.

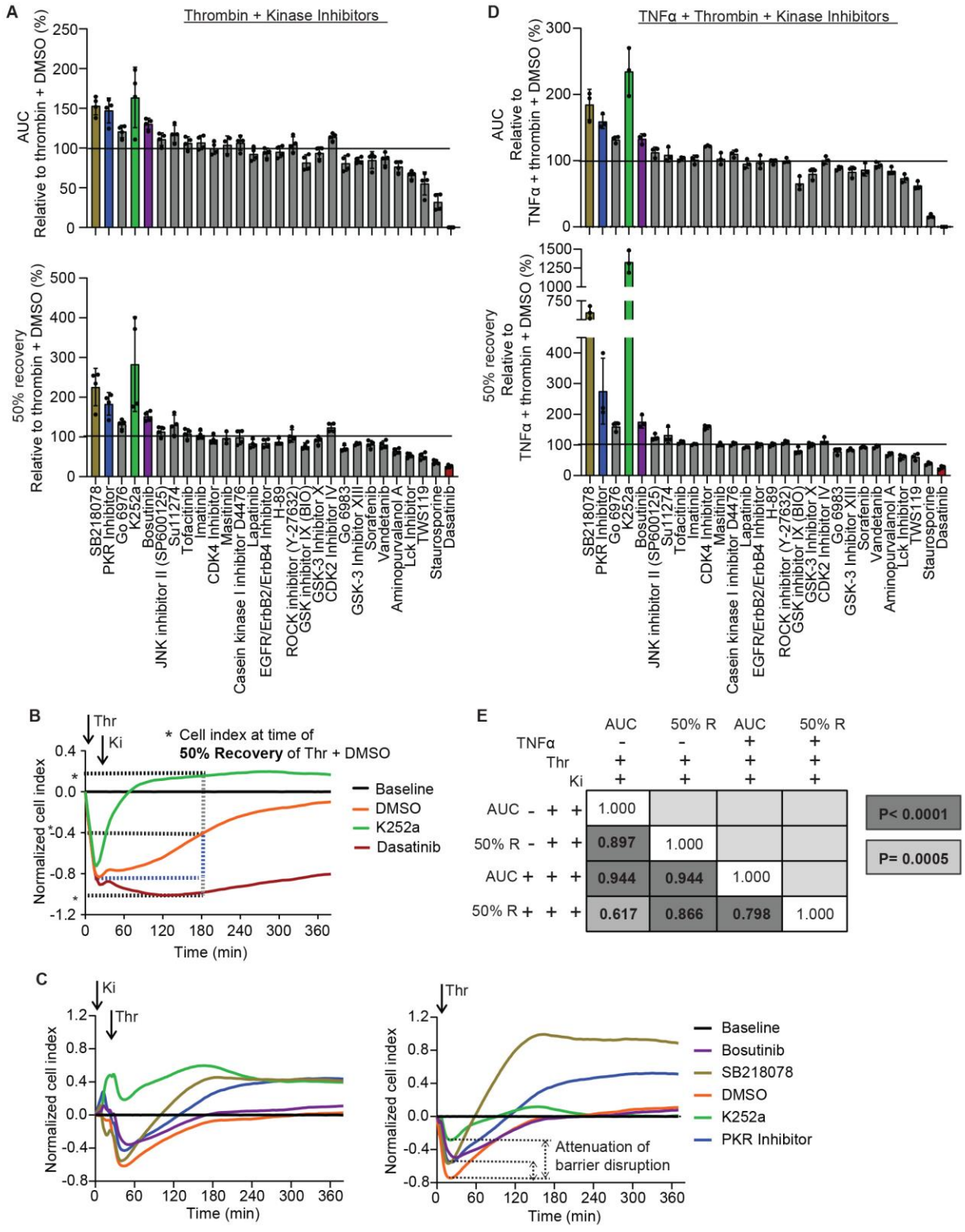

Figure S2. Modulation of HBMEC barrier integrity by kinase inhibitors under inflammatory conditions. Related to Figures 2 and 3.

(A) HBMEC 0.5 μM kinase inhibitor screens in the presence of thrombin.

(B) Representative recording from an xCELLigence assay illustrating the 50% recovery cell index for cells treated with thrombin + DMSO, K252a and dasatinib. Thrombin was added 6 to 9 minutes before kinase inhibitors (Ki).
(C) Left: Representative recording from one of three independent xCELLigence assays in which 0.5 μM kinase inhibitors (Ki) were added to HBMECs for 15-20 min before the addition of 5 nM thrombin. Right: The same xCELLigence recordings normalized to the timepoint before addition of thrombin. Prior treatment with kinase inhibitors attenuates thrombin-induced barrier disruption.
(D) HBMEC 0.5 μM kinase inhibitor screens in the presence of TNFα + thrombin
(A and D) Top graphs: AUC; Bottom graphs: 50% recovery. Data represent the mean ± SD of 4 biological replicates (A), or 3 biological replicates (D), each in triplicate. The DMSO control in each instance is set to 100%.
(E) Correlation between the mean AUC and 50% recovery measurements for HBMECs treated with kinase inhibitors in the three conditions (resting, thrombin, or TNFα + thrombin). The Pearson correlation coefficients and associated *P*-values are determined for measurements with the 28 kinase inhibitors over the entire time course of assays.

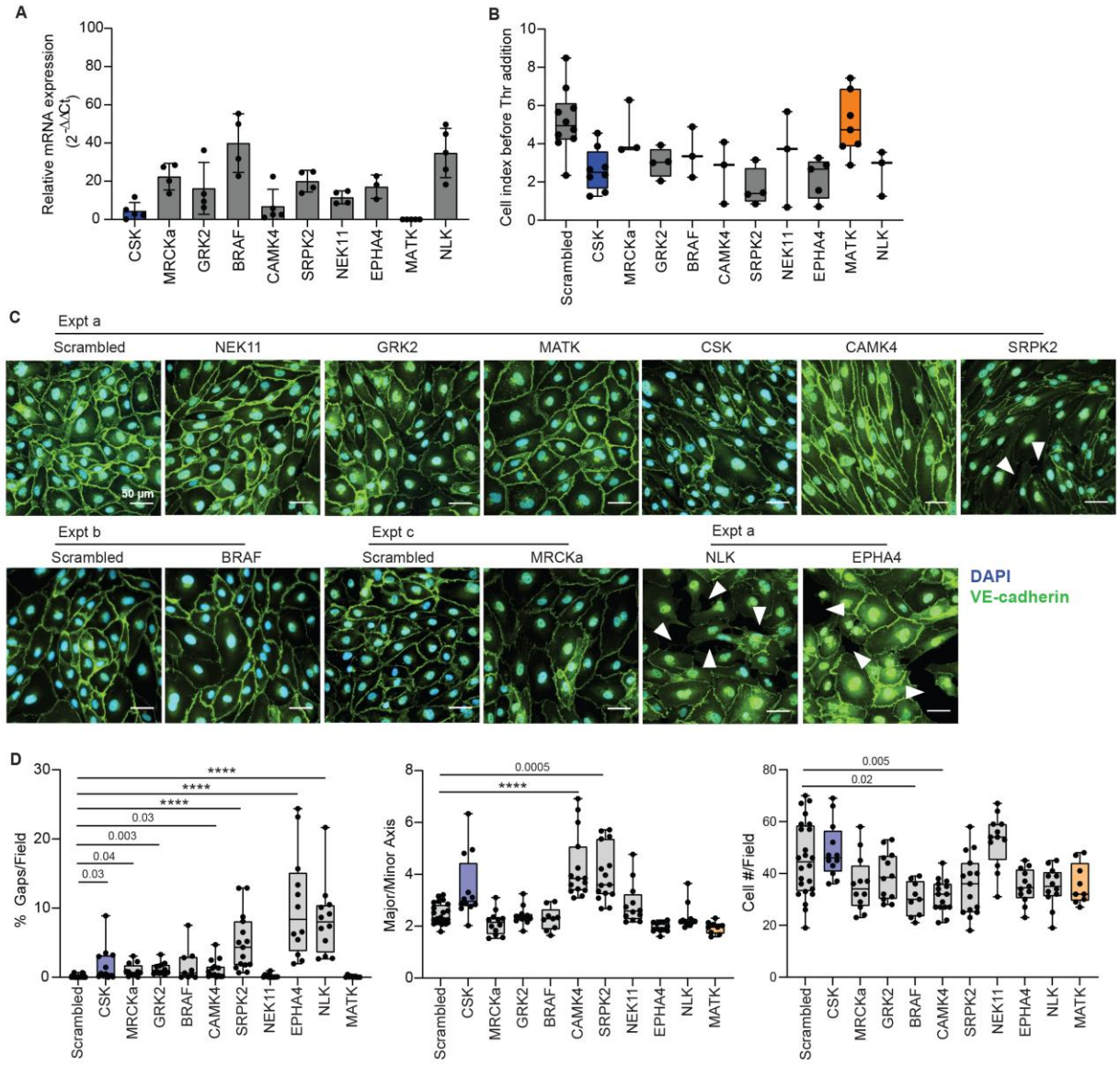

Figure S3. Effect of kinase knockdowns in resting HBMECs. Related to Figure 5.
(A) mRNA expression of kinases after shRNA knockdown. Kinase expression was determined by quantitative RT-PCR and normalized to expression in the scrambled control. Data represent the mean ± SD of 3-5 independent experiments. Black circles represent independent experiments. MATK expression was depleted to levels below detection.
(B) Cell index at the time point before addition of 5 nM thrombin in xCELLigence assays of kinase knockdown cells. The box and whisker plots show the median, 25th and 75th percentiles of 3-10 independent experiments. The whiskers extend to the maximum and minimum values. Black circles represent independent experiments.
(C) Images of kinase knockdown cells and scrambled control cells in the resting state. The images are representative of 3-8 independent experiments and are taken from 3 experiments (a, b, c). Arrowheads indicate gaps. Scale bars: 50 µm.
(D) Quantification of intercellular gaps, cell aspect ratio (major/minor axis) and cell number in images of kinase knockdown and control cells in the resting state. Three fields were analyzed per

experimental condition in each of 3-8 independent experiments. Black circles represent each field. Box and whisker plots show the median, 25^{th} and 75^{th} percentiles. Statistical significance between scrambled and knockdown cells was evaluated using Kruskal-Wallis and Dunn's multiple comparison test (****$P < 0.0001$).

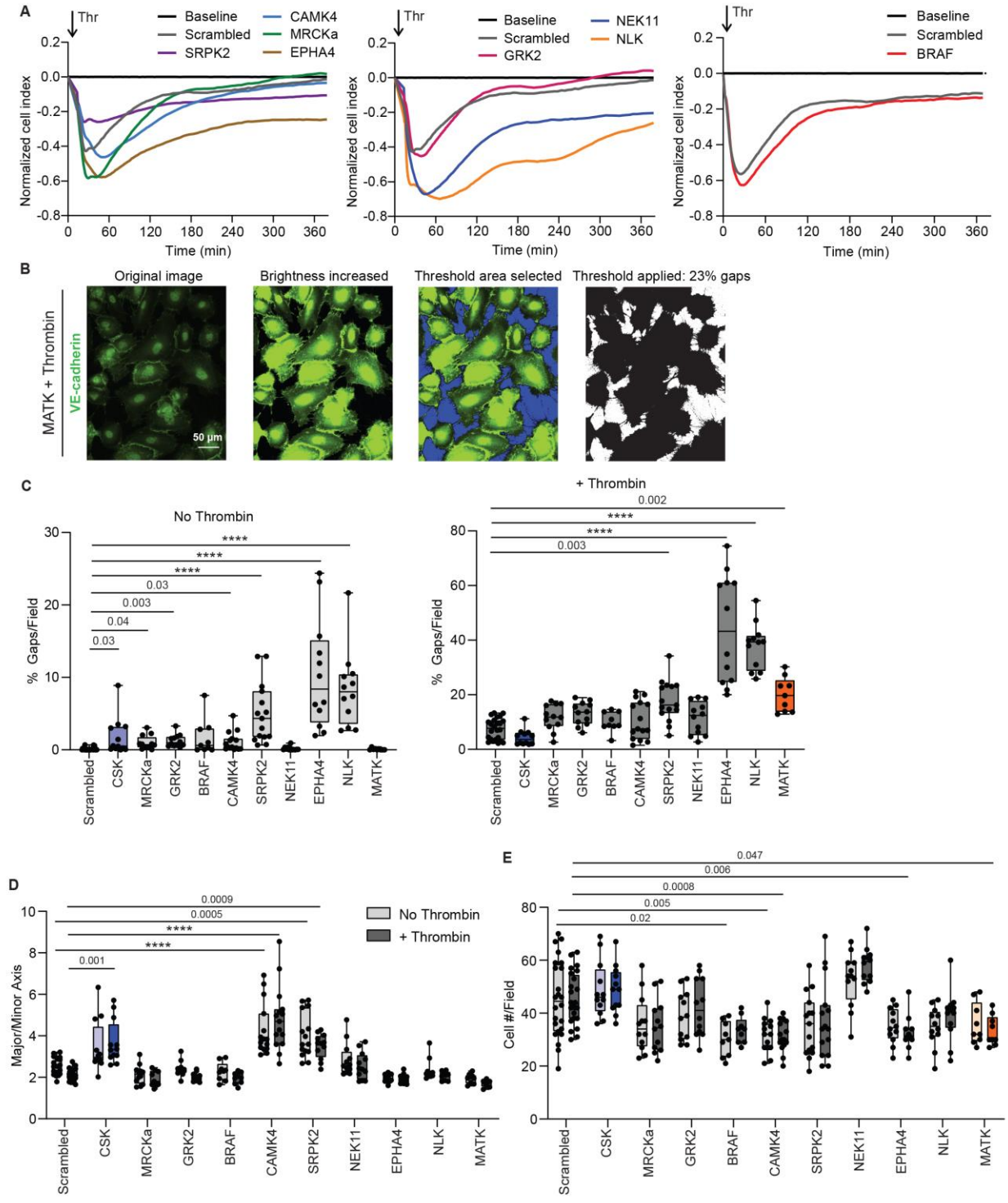

Figure S4. Characterization of kinase knockdown HBMECs in resting and thrombin-activated conditions. Related to Figure 5.

(A) Representative recordings from xCELLigence assays showing the response of each kinase knockdown cell line to thrombin over the course of 360+ min. The left and middle graphs are from one experiment and the right graph is from another.

(B) Illustration of ImageJ gap quantification method in MATK knockdown cells treated with 5 nM thrombin for 40 min. Scale bar: 50 μm.
(C-E) ImageJ quantification of images of kinase knockdown cells in the resting state or 40 min after addition of thrombin showing intercellular gaps (C), cell aspect ratio (D), and cell number (E). Data from cells in the resting state are reproduced from Figure S3D for easy comparison with thrombin-activated cells. Three fields were analyzed per experimental condition in 3-8 independent experiments. The box and whisker plots show the median, 25^{th} and 75^{th} percentiles. Whiskers extend to the maximum and minimum values. Statistical significance between scrambled control cells and all other knockdowns in either the resting state or under thrombin stimulation was evaluated using Kruskal-Wallis and Dunn's multiple comparison test (****$P <$ 0.0001).

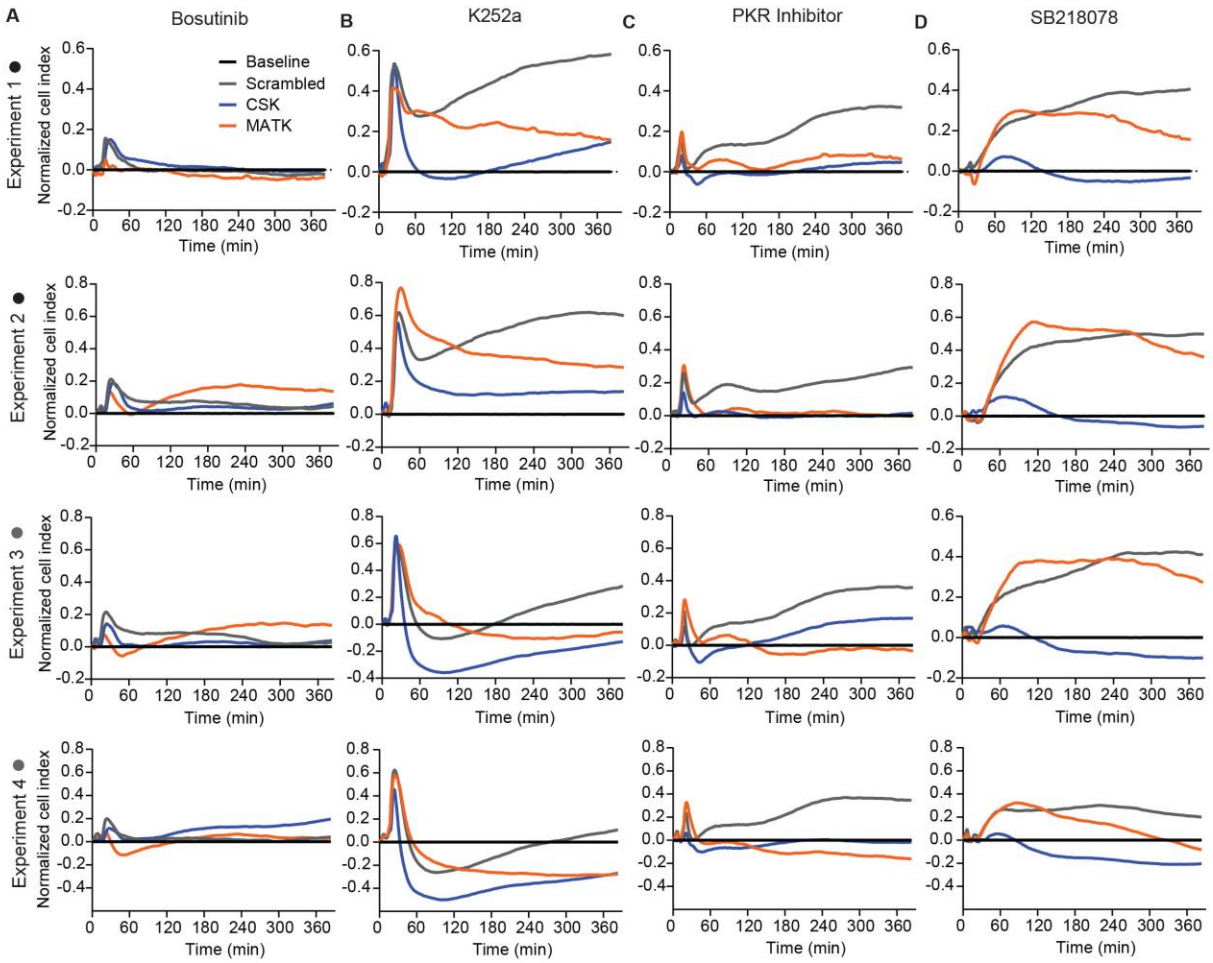

Figure S5. Differential contribution of CSK and MATK to the protective activity of kinase inhibitors. Related to Figure 6.

Recordings from four independent xCELLigence assays showing the normalized cell index after addition of kinase inhibitors to scrambled control, CSK knockdown and MATK knockdown HBMECs. K252a did not induce the sustained barrier-enhancing effect in experiments 3 and 4.

Table S1. Kinase inhibitors used in HBMEC screens. Related to Figures 2 and 3.

#	Kinase Inhibitor	CAS Number
1	Aminopurvanolol A	220792-57-4
2	Bosutinib	380843-75-4
3	Casein kinase I inhibitor D4476	301836-43-1
4	CDK2 inhibitor IV; NU6140	444723-13-1
5	CDK4 inhibitor	546102-60-7
6	Dasatinib	302962-49-8
7	EGFR/ErbB2/ErbB4 inhibitor	881001-19-0
8	Go 6976	136194-77-9
9	Go 6983	133053-19-7
10	GSK-3 inhibitor IX (BIO)	667463-62-9
11	GSK-3 Inhibitor X	740841-15-0
12	GSK-3 Inhibitor XIII	404828-08-6
13	H89	130964-39-5
14	Imatinib	152459-95-5
15	JNK inhibitor II (SP600125)	129-56-6
16	K252a	99533-80-9
17	Lapatinib	388082-78-8
18	Lck inhibitor	213743-31-8
19	Masitinib	790299-79-5
19[a]	JAK inhibitor I	457081-03-7
20	PKR inhibitor	608512-97-6
21	ROCK inhibitor (Y-27632)	129830-38-2
22	SB 218078	135897-06-2
23	Sorafenib	284461-73-0
24	Staurosporine	62996-74-1
25	SU11274	658084-23-2
26	Tofacitinib	477600-75-2
27	TWS119	601514-19-6
28	Vandetanib	443913-73-3

[a]JAK inhibitor I was used in place of masitinib in a single replicate of the HBMEC + thrombin screen.

Table S3. Identifying information for shRNA clones used in kinase knockdowns. Related to Figure 5 and STAR Methods.

Gene Symbol	Gene Description	Sigma MISSION shRNA Clone ID[a]
ADRBK1	adrenergic, beta, receptor kinase 1	TRCN0000000559
ADRBK1	adrenergic, beta, receptor kinase 1	TRCN0000000560
ADRBK1	adrenergic, beta, receptor kinase 1	TRCN0000000561
BRAF	v-raf murine sarcoma viral oncogene homolog B1	TRCN0000231130
BRAF	v-raf murine sarcoma viral oncogene homolog B1	TRCN0000196844
CAMK4	calcium/calmodulin-dependent protein kinase IV	TRCN0000000577
CAMK4	calcium/calmodulin-dependent protein kinase IV	TRCN0000000578
CDC42BPA	CDC42 binding protein kinase alpha (DMPK-like)	TRCN0000000659
CDC42BPA	CDC42 binding protein kinase alpha (DMPK-like)	TRCN0000000660
CDC42BPA	CDC42 binding protein kinase alpha (DMPK-like)	TRCN0000000661
CSK	c-src tyrosine kinase	TRCN0000000804
NEK11	NIMA (never in mitosis gene a)- related kinase 11	TRCN0000001961
NEK11	NIMA (never in mitosis gene a)- related kinase 11	TRCN0000001962
NEK11	NIMA (never in mitosis gene a)- related kinase 11	TRCN0000001963
MATK	megakaryocyte-associated tyrosine kinase	TRCN0000002222
SRPK2	SFRS protein kinase 2	TRCN0000006277
NLK	nemo-like kinase	TRCN0000002069
EPHA4	EPH receptor A4	TRCN0000010165

[a]Optimal knockdown was achieved with either 1, 2 or 3 shRNA targeting constructs.

Table S4. Primer sequences for qPCR quantification of kinase expression. Related to Figure 5 and STAR Methods.

Kinase	Accession number	PrimerBank ID[a]	Forward	Reverse
BRAF	P15056	187608632c1	AATACACCAGCAAGCTAGATGC	AATCAGTTCCGTTCCCCAGAG
CAMK4	Q16566	312596937c1	GCCTCGTCCCGGATTACTG	TCCCCTTCTGTTTGCATCTGT
CSK	P41240	187475372c2	TTCCACGGCAAGATCACACG	GCATGGTACATGATGCGGTAG
EPHA4	P54764	45439363c1	TTCGCCCTATTTTCGTGTCTC	TGGTAGGTTCGGATTGGTGTAT
GRK2 (ADRBK1)	P25098	148539875c1	TCCAGCCATACATCGAAGAGA	CAAAACCGTGTGAACTTATCGC
MATK (CTK)	P42679	111159470c2	TTGGGAGCACAGATCGGAGA	GGGCTGTCACATCACACTTGA
MRCKa (CDC42BPA)	Q5VT25	113204433c3	TGGAACGGTTCAGTCCTCAGT	TATGTCTCCACCAGCGATTCT
NEK11	Q8NG66	225637561c3	ACAGAAAATGACGCCAAGAGAA	AGCTGCTGAAAGTTCCGAGAT
NLK	Q9UBE8	149408125c3	CCAACCTCCACACATTGACTATT	ACTTTGACATGATCTGAGCTGAG
SRPK2	P78362	33188446c2	ACATGGTGGTCCAGCTCATTG	CTCTTCACACAACGTACTGGG
GAPDH	P04406	378404907c1	GGAGCGAGATCCCTCCAAAAT	GGCTGTTGTCATACTTCTCATGG
ACTB	P60709	4501885a1	CATGTACGTTGCTATCCAGGC	CTCCTTAATGTCACGCACGAT

[a]Primer sequences were obtained from PrimerBank: https://pga.mgh.harvard.edu/primerbank/